Supporting Information

Flexible Luminescent MOF: Trapping of Less Stable Conformation of Rotational Isomers, In Situ Guest Responsive Turn-Off and Turn-On Luminescence and Mechanistic Study

Sajal Khatua*[a] and Protap Biswas[a].
[a] School of Chemical Sciences, Indian Association for the Cultivation of Science, 2A & 2B Raja S. C. Mullick Road, Kolkata-700032, West Bengal., India.
Email: ocsk2@iacs.res.in

Experimental Section:

Selectivity Test for Encapsulation of Volatile Organic Solvents: The orange crystals (120 mg) of the parent MOF (**1**) in 5 mL small open vial were placed in to 20ml capped vials containing a mixture of $CHCl_3$, CH_2Cl_2 and CCl_4 with a volume ratio 1:1:1 for vapor diffusion for 7 days. Solvent-exchanged crystals suitable for X-ray diffraction were obtained.

Reversibility Test for volatile Organic Solvent Encapsulation: When activated sample (**1′**) was exposed for vapour ($CHCl_3$, CH_2Cl_2 and CCl_4) diffusion for 7 days at RT, the volatile organic solvents were incorporated in the void space to yield **1n'**, **1o'** and **1p'** which are identical to **1n**, **1o** and **1p,** respectively (Scheme S1). The appearance of the characteristic FTIR peaks for respective volatile organic solvents in 1D channel of **1n'**, **1o'** and **1p'** confirmed that those peaks were also present in **1n**, **1o** and **1p,** respectively (**1n'**, **1o'** and **1p'** identical to **1n**, **1o** and **1p,** respectively) (Figure S12 (b-d)). The RT PXRD patterns of **1n'**, **1o'** and **1p'** suggested that the basic framework architecture of **1** was retained after incorporation of volatile organic solvent molecules (Figure S12 (e)). The empty framework architecture of **1′** can be regenerated by simple heating the solvent exchanged complexes (**1n'**, **1o'** and **1p'**) at 160 °C for 24 h (Scheme S1) which confirmed its reversibility.

Selectivity Test for Encapsulation of Rotational Isomers: The insoluble crystals of **1** in small (5ml) open glass vial were kept into capped glass vial (20 mL) containing a mixture of DCE, DBE and ethylene glycol with a volume ratio 1:1:1 for 7 days.

Reversibility Test for Encapsulation of Rotational Isomers: The same method as for the reversible encapsulation of volatile organic solvents was followed but here, **1'** was exposed for vapor diffusion in different rotational vapors (DCE, DBE and ethylene glycol) for 7 days at room temperature. The rotational isomer included complexes (**1q'**, **1r'**, and **1s'**) were confirmed by characteristic FT-IR peaks as found in **1q, 1r** and **1s**, respectively (Scheme S2 and Figure S18 (a-c)). The PXRD patterns of **1q'**, **1r'** and **1s'** suggested that

the basic framework pattern of **1** was remained the same after incorporation of rotational isomers but some peaks appear at lower angles (Figure S18 (d)). This might be due to mechanical sliding of the interpenetrated 2D sheet structures of **1**. By heating of **1q'**, **1r'** and **1s'** at 160 °C for 24 h, **1′** can be regenerated (Scheme S2) which confirmed its reversible inclusion of rotational isomers by Cu(I)MOF.

Selectivity Test for Encapsulation of benzene and its derivatives and naphthalene: The same method as for the selective test for volatile organic solvents was followed but here MeCN solution of naphthalene was mixed with a mixture of benzene and its derivatives in a volume ratio of 1:1:1:1:1:1 and **1** was kept for vapor diffusion in this vapour mixture for 7 days at rt.

Reversibility Test for Encapsulation of benzene and its derivatives and naphthalene: The same procedure as for reversible encapsulation of volatile organic solvents was followed but **1'** was kept for vapor diffusion of benzene and its derivatives and naphthalene (naphthalene in MeCN solution) separately for a period of 7 days at RT. The benzene and its derivatives and naphthalene included complexes (**1t**', **1u**', **1v**', **1w**', **1x**'and **1y**') were confirmed by characteristic FT-IR peaks as found in **1t**, **1u**, **1v**, **1w**, **1x** and **1y**, respectively (Figure S28 (a-f)). PXRD patterns of **1t**', **1u**', **1v**', **1w**', **1x**'and **1y**' indicated that the basic framework architecture of **1** was remained the same but, some peaks appear at lower angle (Figure S28(g-h)). This can be attributed to mechanical sliding of the interpenetrated 2D sheet structures of **1**. By heating of **1t**', **1u**', **1v**', **1w**', **1x**' and **1y**'at 160 °C for 24 h, **1′** can be regenerated (Scheme S4) which confirmed its reversible inclusion of benzene and its derivatives and naphthalene by Cu(I)MOF.

Isolation of intermediate of each guest encapsulation: Orange crystals of **1** were exposed to vapors of $CHCl_3$, CH_2Cl_2, CCl_4, DCE, DBE, ethylene glycol, PhH, $PhCH_3$, *o*-$PhCl_2$, $PhNH_2$, $PhCH_2NH_2$ and naphthalene (in MeCN soln.) for a weak at room temperature. To investigate mechanism behind inclusion process, we stopped the reaction after three days for each guest inclusion process and isolated the intermediate of each guest inclusion. The intermediate was appeared as black material and suitable for SXRD analysis.

Hot stage microscopic image experiment: In one set of experiment, one single crystal of **1** was heated from 25 to 200 ^{o}C and per 10°C rise in temperature we collected the change in color of **1**. In another set of experiment, at transient temperature where orange color crystal turned into black crystal, was collected for SCXRD analysis.

Photoluminescence (PL) Study of all guest exchanged complexes in Solid Phase: Orange crystal of **1** (120 mg each) were exposed to vapor of different volatile organic solvents ($CHCl_3$, CH_2Cl_2 and CCl_4), rotational isomers (DCE, DBE and ethylene glycol), benzene and its derivatives and naphthalene (MeCN soln.) for 7 days. PL data of the guest included compounds were recorded at room temperature upon excitation at 418 nm.

PL Study of the benzene and its derivatives in Solution Phase: 1.0 mM saturated solution of each analyte was prepared in 10 mL dry MeCN. 1 mg of **1** was added to 3 mL of dry MeCN under stirring. The fluorescence was measured in-situ in the range of 300-535 nm upon addition of freshly prepared analyte solutions (λ_{ex} = 268 nm). Solutions were stirred at constant rate during experiment to make a homogenous solution. All the experiments were performed in triplicate and consistent results are obtained in all cases.

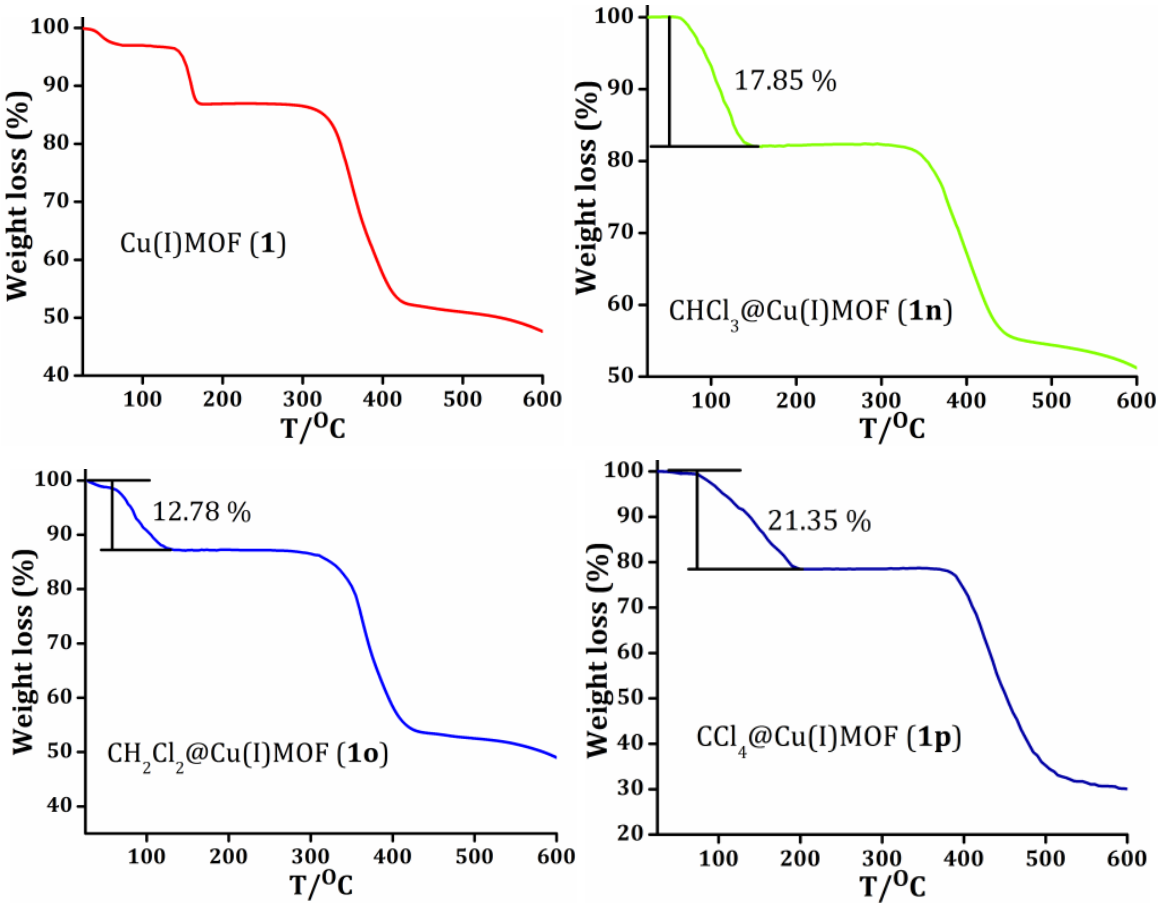

Figure S1. TGA plots of **1** and all the volatile organic solvent included complexes.

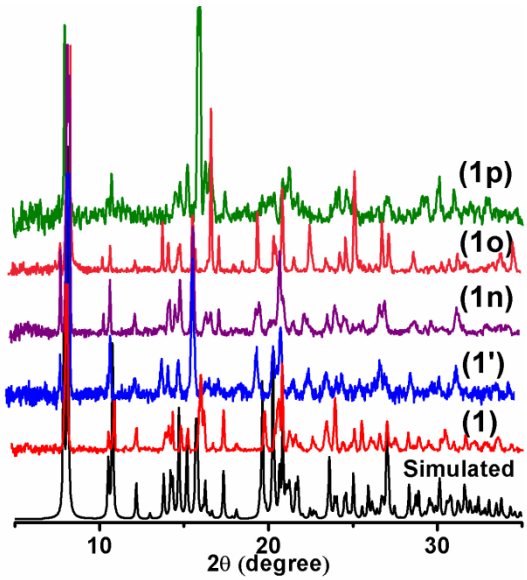

Figure S2. PXRD patterns of the simulated, as-synthesized (**1**), activated (**1'**) and different volatile organic solvent included complexes.

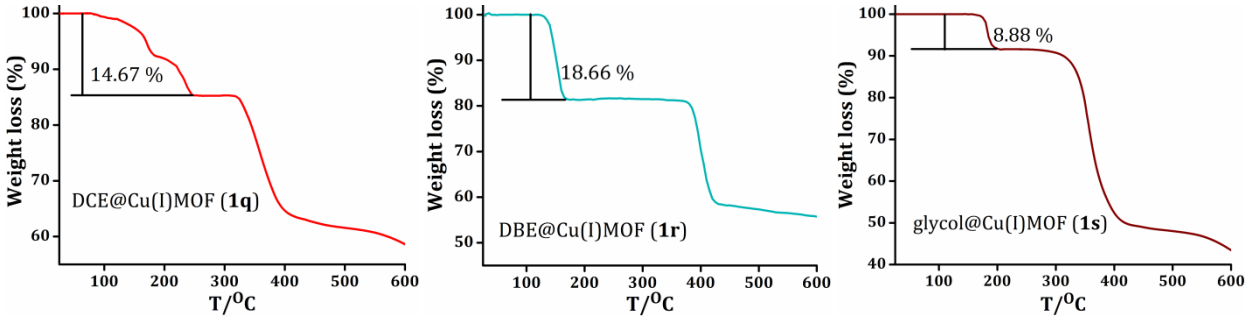

Figure S3. TGA plots of all the rotational isomer included complexes.

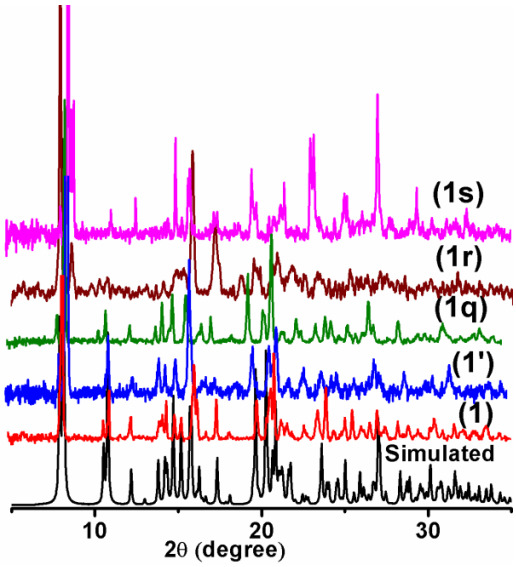

Figure S4. PXRD patterns of the simulated, as-synthesized (**1**), activated (**1'**) and different rotational isomers included complexes.

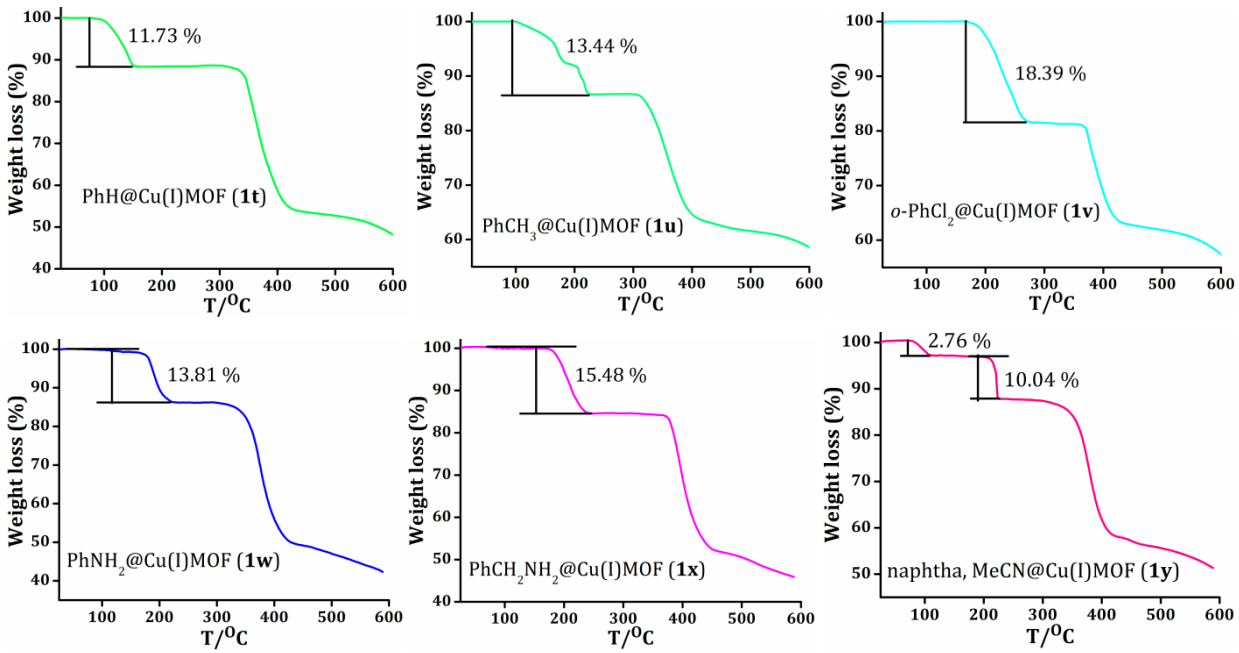

Figure S5. TGA plots of all benzene and its derivatives, and naphtha included complexes.

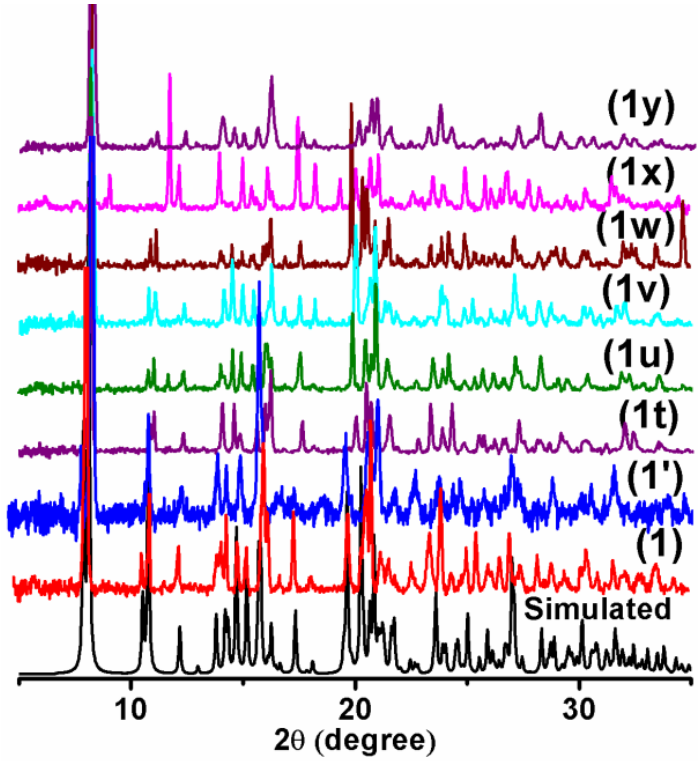

Figure S6. PXRD patterns of the simulated, as-synthesized (**1**), activated (**1'**), benzene and its derivatives and naphthalene included complexes.

Table S1. Crystal and structure refinement data for guest included Cu(I)MOF.

Identification code	**1n**	**1o**	**1p**	**1q**
CCDC No	**1918497**	**1918499**	**1918500**	**1918498**
Empirical formula	$C_{46}H_{36}Cl_6Cu_2I_2N_6O_2$	$C_{23}H_{19}Cl_2CuIN_3O$	$C_{23}H_{15.95}Cl_4CuIN_3O$	$C_{48}H_{42}Cl_4Cu_2I_2N_6O_2$
Formula weight	1298.39	614.75	682.57	1257.55
Temperature/K	100	100	100	100
Crystal system	triclinic	monoclinic	monoclinic	monoclinic
Space group	*P-1*	*C2/c*	*C2/c*	*C2/c*
a/Å	12.166(4)	24.6615(9)	24.282(3)	25.122(3)
b/Å	13.376(5)	12.0846(5)	12.4370(14)	11.9422(11)
c/Å	18.035(5)	18.0322(7)	17.961(2)	17.937(2)
α/°	68.76(2)	90	90	90
β/°	74.17(2)	113.580(2)	112.100(4)	113.817(5)
γ/°	66.27(2)	90	90	90
Volume/$Å^3$	2476.5(15)	4925.3(3)	5025.5(10)	4922.9(9)
Z	2	8	8	4
ρ_{calc}g/cm^3	1.741	1.658	1.804	1.697
μ/mm^{-1}	2.473	2.377	2.545	2.38
F(000)	1272	2416	2664	2480
Crystal size/mm^3	0.36 × 0.35 × 0.34	0.36 × 0.35 × 0.32	0.56 × 0.53 × 0.45	0.45 × 0.23 × 0.2
Radiation	MoKα (λ = 0.71073)	MoKα (λ = 0.71073)	MoKα (λ = 0.71073)	MoKα (λ = 0.71073)
2Θ range for data collection/°	2.45 to 50.876	3.604 to 50.698	4.082 to 50.952	3.844 to 51.968
Index ranges	$-13 \le h \le 14$, $-14 \le k \le 16$, $0 \le l \le 21$	$-29 \le h \le 29$, $-14 \le k \le 14$, $-21 \le l \le 21$	$-25 \le h \le 29$, $-15 \le k \le 14$, $-21 \le l \le 21$	$-30 \le h \le 30$, $-14 \le k \le 14$, $-17 \le l \le 21$
Reflections collected	8187	34629	21459	15735
Independent reflections	8187 [R_{int} = 0.0756, R_{sigma} = 0.1345]	4515 [R_{int} = 0.0721, R_{sigma} = 0.0405]	4644 [R_{int} = 0.0511, R_{sigma} = 0.0425]	4628 [R_{int} = 0.0377, R_{sigma} = 0.0336]
Data/restraints/parameters	8187/0/556	4515/0/269	4644/1/348	4628/0/290
Goodness-of-fit on F^2	1.228	1.157	1.266	1.094
Final R indexes [I>=2σ (I)]	R_1 = 0.1083, wR_2 = 0.2767	R_1 = 0.1075, wR_2 = 0.2353	R_1 = 0.0983, wR_2 = 0.2325	R_1 = 0.0554, wR_2 = 0.1333
Final R indexes [all data]	R_1 = 0.2030, wR_2 = 0.3533	R_1 = 0.1354, wR_2 = 0.2519	R_1 = 0.1089, wR_2 = 0.2385	R_1 = 0.0719, wR_2 = 0.1486
Largest diff. peak/hole / e $Å^{-3}$	3.51/-1.86	3.60/-1.42	2.02/-2.92	1.60/-1.72

Table S2. Crystal and structure refinement data for guest included Cu(I)MOF.

Identification code	**1r**	**1s**	**1t**	**1u**
CCDC No	**1918502**	**1918504**	**1918507**	**1918501**
Empirical formula	$C_{24}H_{19}Br_{1.25}CuIN_3O$	$C_{24}H_{22}CuIN_3O_3$	$C_{28}H_{22}CuIN_3O$	$C_{29}H_{24}CuIN_3O$
Formula weight	655.75	590.88	606.92	620.95
Temperature/K	100	100	100	100
Crystal system	monoclinic	monoclinic	monoclinic	monoclinic
Space group	*C2/c*	*I2/c*	*C2/c*	*C2/c*
a/Å	24.3244(9)	18.180(2)	23.696(4)	23.8568(9)
b/Å	12.2780(5)	11.8500(10)	12.9253(19)	12.7232(5)
c/Å	17.7756(6)	24.082(3)	17.710(3)	17.6759(7)
α/°	90	90	90	90
β/°	112.772(2)	109.299(8)	111.762(2)	112.562(2)
γ/°	90	90	90	90

Volume/Å^3	4895.0(3)	4896.5(9)	5037.4(13)	4954.6(3)
Z	8	8	8	8
ρ_{calc}g/cm^3	1.78	1.603	1.601	1.665
μ/mm^{-1}	4.215	2.182	2.118	2.156
F(000)	2542	2344	2408	2472
Crystal size/mm^3	0.35 × 0.25 × 0.2	0.25 × 0.24 × 0.23	0.42 × 0.23 × 0.21	0.18 × 0.15 × 0.12
Radiation	MoKα (λ = 0.71073)	MoKα (λ = 0.71073)	MoKα (λ = 0.71073)	MoKα (λ = 0.71073)
2Θ range for data collection/°	3.632 to 50.896	3.876 to 51.484	3.654 to 53.464	3.696 to 56.754
Index ranges	-29 ≤ h ≤ 29, -14 ≤ k ≤ 14, -21 ≤ l ≤ 21	-21 ≤ h ≤ 21, -14 ≤ k ≤ 14, -27 ≤ l ≤ 29	-29 ≤ h ≤ 29, -16 ≤ k ≤ 16, -22 ≤ l ≤ 22	-29 ≤ h ≤ 29, -16 ≤ k ≤ 16, -22 ≤ l ≤ 22
Reflections collected	25810	40513	62642	6150
Independent reflections	4524 [R_{int} = 0.0573, R_{sigma} = 0.0461]	4584 [R_{int} = 0.1277, R_{sigma} = 0.0583]	5359 [R_{int} = 0.0399, R_{sigma} = 0.0187]	6150 [R_{int} = 0.064, R_{sigma} = 0.0414]
Data/restraints/parameters	4524/1/276	4584/1/266	5359/0/269	6150/1/296
Goodness-of-fit on F^2	1.043	1.168	1.071	1.074
Final R indexes [I>=2σ (I)]	R_1 = 0.1049, wR_2 = 0.2730	R_1 = 0.1348, wR_2 = 0.2927	R_1 = 0.0641, wR_2 = 0.1358	R_1 = 0.0457, wR_2 = 0.1227
Final R indexes [all data]	R_1 = 0.1396, wR_2 = 0.3033	R_1 = 0.1494, wR_2 = 0.3017	R_1 = 0.0810, wR_2 = 0.1507	R_1 = 0.0633, wR_2 = 0.1341
Largest diff. peak/hole / e Å^{-3}	4.49/-3.43	2.51/-3.79	2.15/-1.24	1.15/-1.04

Table S3. Crystal and structure refinement data for guest included Cu(I)MOF.

Identification code	**1v**	**1w**	**1x**
CCDC No	**1918506**	**1918503**	**1918505**
Empirical formula	$C_{28}H_{21}Cl_{1.5}CuIN_3O$	$C_{56}H_{48}Cu_2I_2N_8O_2$	$C_{29}H_{22.64}CuIN_4O$
Formula weight	659.09	1245.9	633.59
Temperature/K	100	100	100
Crystal system	monoclinic	triclinic	monoclinic
Space group	*C2/c*	*P-1*	*C2/c*
a/Å	23.9180(9)	12.5064(12)	24.2935(9)
b/Å	12.7420(5)	13.6759(12)	12.6330(5)
c/Å	17.8041(7)	17.5120(16)	17.7632(6)
α/°	90	109.965(4)	90
β/°	112.848(2)	89.613(4)	113.0070(10)
γ/°	90	114.963(4)	90
Volume/Å^3	5000.3(3)	2518.8(4)	5017.9(3)
Z	8	2	8
ρ_{calc}g/cm^3	1.751	1.643	1.677
μ/mm^{-1}	2.296	2.121	2.131
F(000)	2604	1240	2517
Crystal size/mm^3	0.45 × 0.35 × 0.3	0.45 × 0.4 × 0.4	0.35 × 0.25 × 0.25
Radiation	MoKα (λ = 0.71073)	MoKα (λ = 0.71073)	MoKα (λ = 0.71073)
2Θ range for data collection/°	3.692 to 51.158	4.074 to 50.742	4.844 to 50.734
Index ranges	-27 ≤ h ≤ 28, -15 ≤ k ≤ 15, -21 ≤ l ≤ 21	-15 ≤ h ≤ 15, -16 ≤ k ≤ 15, 0 ≤ l ≤ 21	-29 ≤ h ≤ 29, -15 ≤ k ≤ 15, -20 ≤ l ≤ 21
Reflections collected	22626	8943	24478
Independent reflections	4660 [R_{int} = 0.0381, R_{sigma} = 0.0311]	8943 [R_{int} = 0.0504, R_{sigma} = 0.0523]	4606 [R_{int} = 0.0674, R_{sigma} = 0.0441]

Data/restraints/parameters	4660/21/287	8943/0/636	4606/1/321
Goodness-of-fit on F^2	1.035	1.109	1.047
Final R indexes [I>=2σ (I)]	R_1 = 0.0812, wR_2 = 0.2275	R_1 = 0.0477, wR_2 = 0.0973	R_1 = 0.0662, wR_2 = 0.1755
Final R indexes [all data]	R_1 = 0.1017, wR_2 = 0.2560	R_1 = 0.0730, wR_2 = 0.1148	R_1 = 0.0779, wR_2 = 0.1907
Largest diff. peak/hole / e $Å^{-3}$	2.22/-2.52	1.44/-1.46	2.10/-4.97

Table S4. Crystal and structure refinement data for guest included Cu(I)MOF.

Identification code	**1y**	**1z**
CCDC No	**1918509**	**1918508**
Empirical formula	$C_{56}H_{45}Cu_2I_2N_7O_2$	$C_{22}H_{17}CuIN_3O_2$
Formula weight	1228.87	545.82
Temperature/K	100	100
Crystal system	monoclinic	monoclinic
Space group	*$P2_1/c$*	*C2/c*
a/Å	23.5760(19)	24.184(10)
b/Å	12.8738(11)	12.642(6)
c/Å	17.7114(14)	17.903(8)
α/°	90	90
β/°	110.880(2)	113.189(4)
γ/°	90	90
Volume/$Å^3$	5022.6(7)	5031(4)
Z	4	8
ρ_{calc}g/cm^3	1.625	1.441
μ/mm^{-1}	2.126	2.114
F(000)	2440	2144
Crystal size/mm^3	0.26 × 0.25 × 0.21	0.23 × 0.21 × 0.2
Radiation	MoKα (λ = 0.71073)	MoKα (λ = 0.71073)
2Θ range for data collection/°	4.6 to 50.742	3.664 to 51.132
Index ranges	$-25 \leq h \leq 28$, $-15 \leq k \leq 15$, $-21 \leq l \leq 21$	$-29 \leq h \leq 24$, $-15 \leq k \leq 15$, $-21 \leq l \leq 21$
Reflections collected	50502	14932
Independent reflections	9191 [R_{int} = 0.0566, R_{sigma} = 0.0447]	4667 [R_{int} = 0.1309, R_{sigma} = 0.1446]
Data/restraints/parameters	9191/0/625	4667/0/272
Goodness-of-fit on F^2	1.091	1.023
Final R indexes [I>=2σ (I)]	R_1 = 0.0817, wR_2 = 0.1677	R_1 = 0.0729, wR_2 = 0.2030
Final R indexes [all data]	R_1 = 0.1322, wR_2 = 0.2034	R_1 = 0.1894, wR_2 = 0.2534
Largest diff. peak/hole / e $Å^{-3}$	2.16/-1.68	1.32/-0.74

$^a R_1 = \Sigma||Fo| - |Fc||/\Sigma|Fo|$. $^b R_2 = [\Sigma\{w(Fo^2 - Fc^2)^2\}/\Sigma\{w(Fo^2)^2\}]^{1/2}$

Underlying Net topology analysis: The parent MOF contains a Cu_2I_2 cluster with four centered node (4c) and the ligand is two centered node (2c). When we consider Cu_2I_2 as propagating node alone with 2c ligand node it shows (Topological type: hcb; Shubnikov hexagonal plane net/(6,3) Point symbol for net: {6^3} 3-c net; uninodal net) as shown in Figure S7. Then we simplify the Cu_2I_2 as a point that is this cluster were simplified to a point (4c) and ligand was considered as 2c point and the observed topology is Topological type: (sql/Shubnikov tetragonal plane net Point symbol for net: {4^4.6^2} 4-c net; uninodal net) (Figure S8).

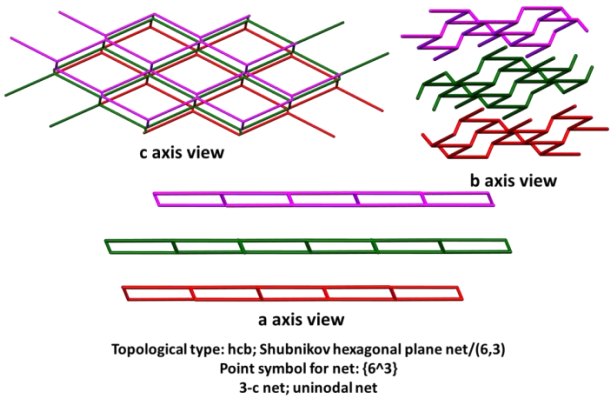

Figure S7. Topological analysis of the parent MOF (**1**) before cluster simplification.

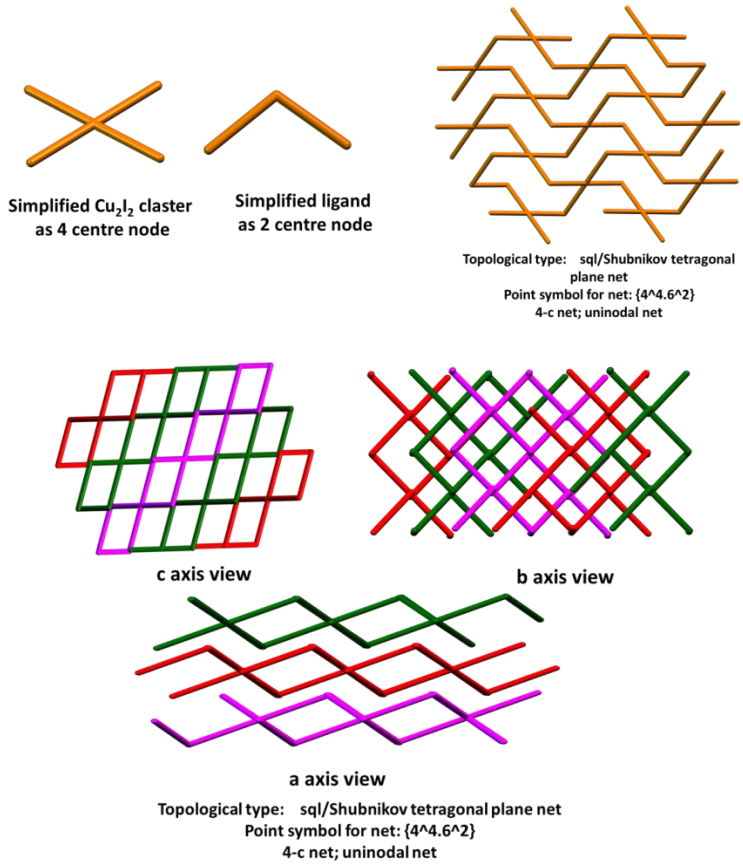

Figure S8. Topological analysis of the parent MOF (**1**) after cluster simplification.

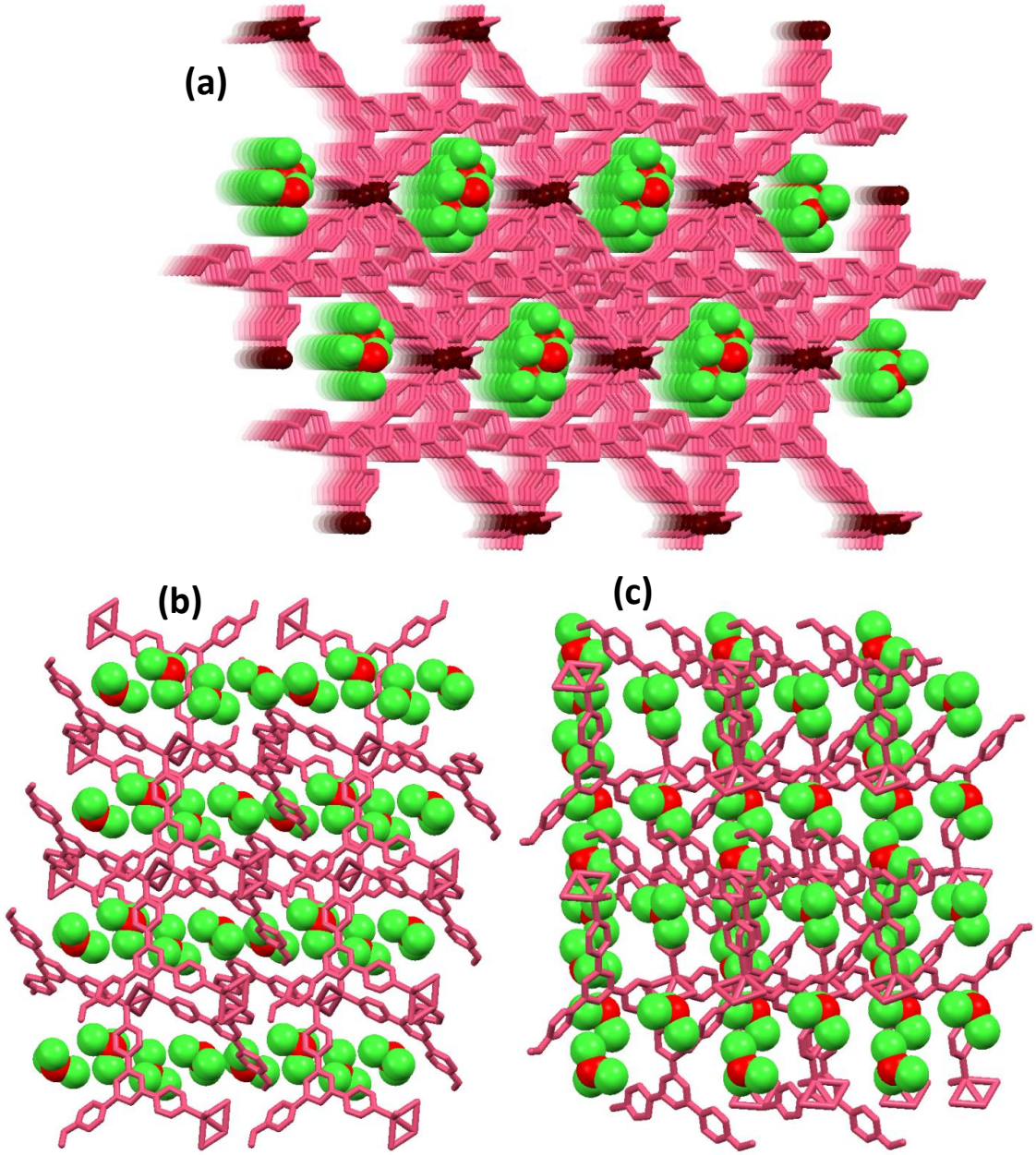

Figure S9. Solid state packing diagram of **$CHCl_3$** molecules in **$CHCl_3$@Cu(I)MOF** (a) down the *C-axis*; (b)-(c) zigzag arrangement of **$CHCl_3$** molecules along the *b* and *c*-axes.

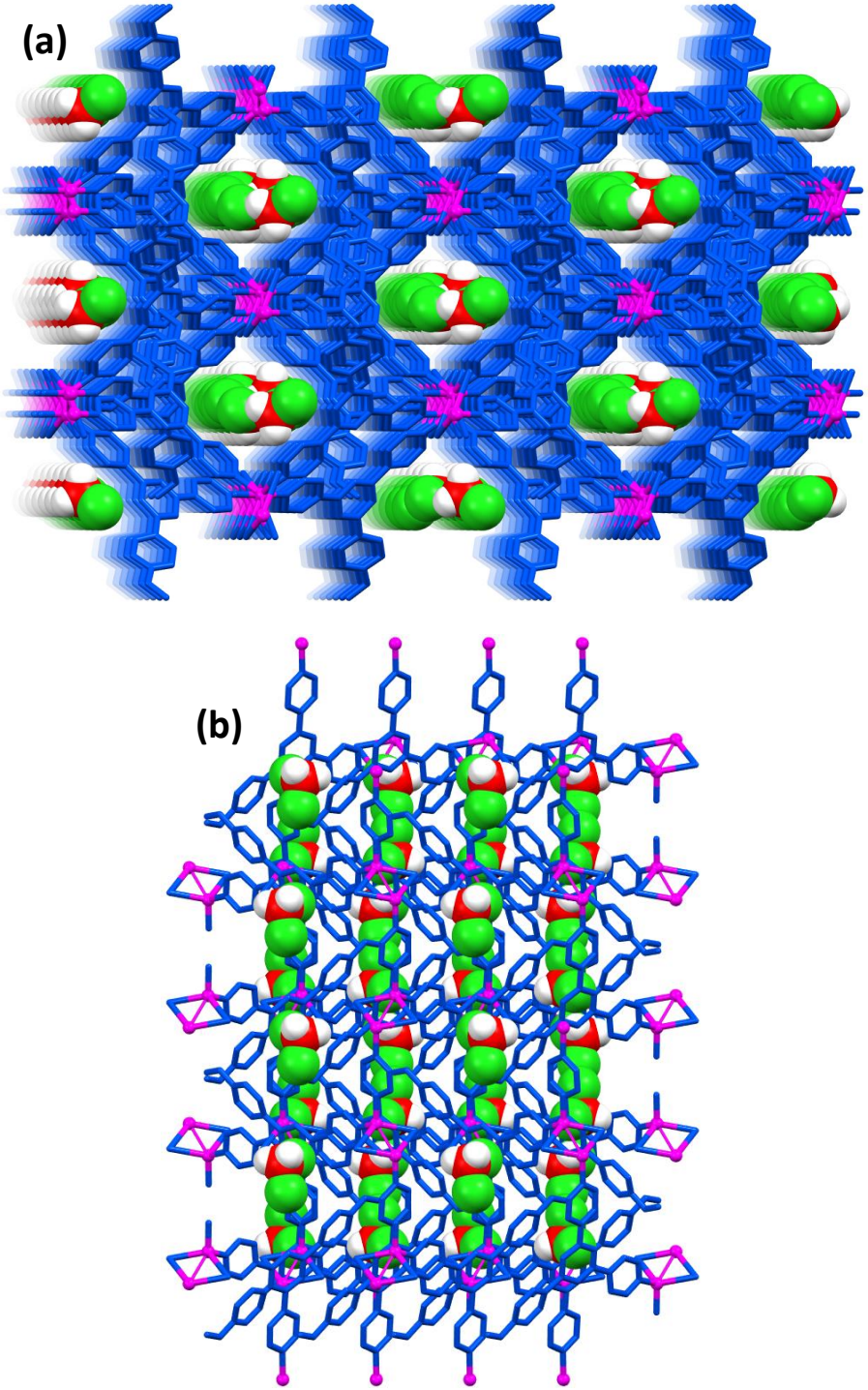

Figure S10. Solid state packing diagram of **CH_2Cl_2** molecules in **CH_2Cl_2@Cu(I)MOF** (a) down the *c-axis*; (b) zigzag arrangement of **CH_2Cl_2** molecules along the *b*-axis.

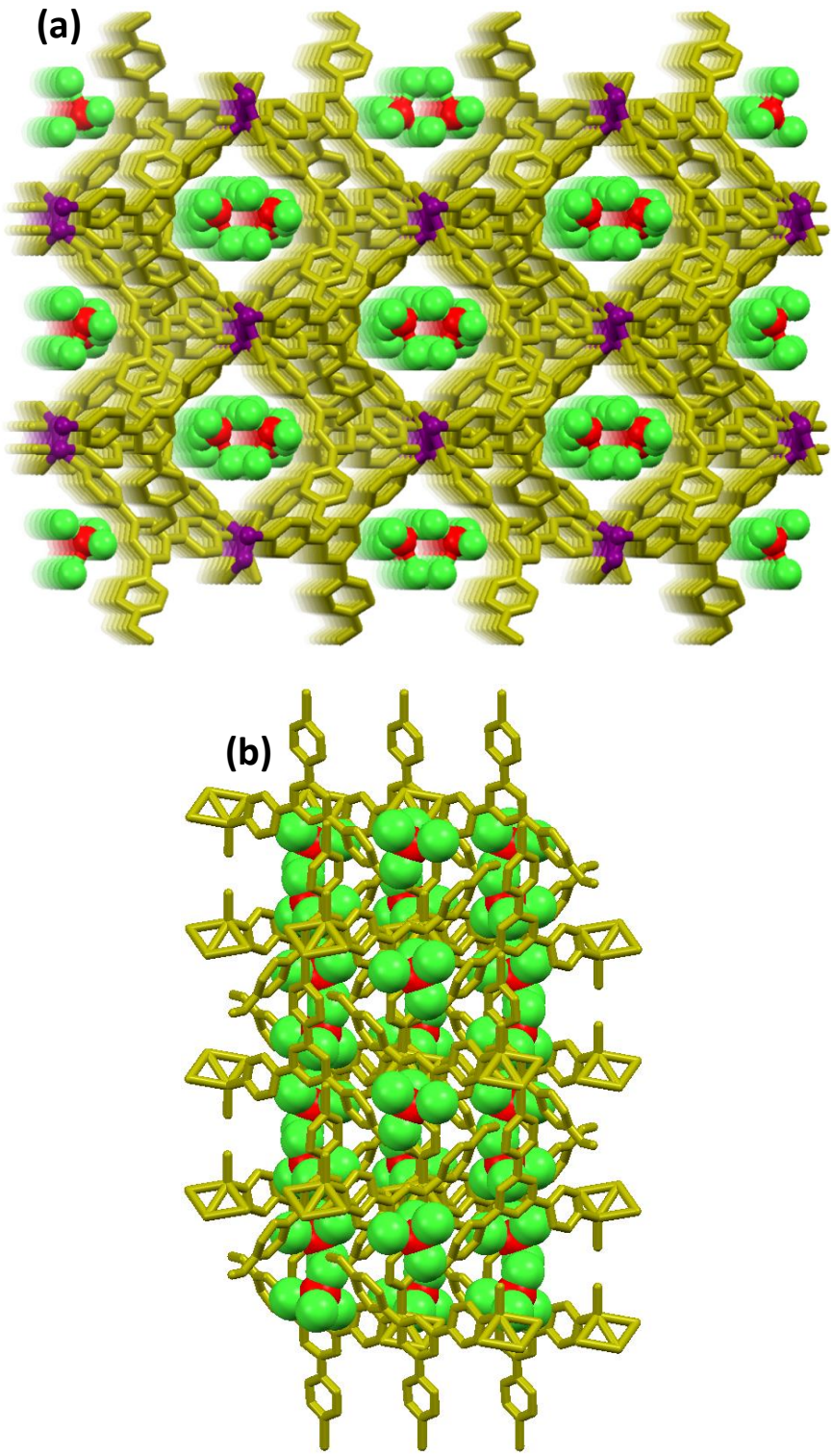

Figure S11. Solid state packing diagram of **CCl_4** molecules in **CCl_4@Cu(I)MOF** (a) down the *c-axis*; (b) zigzag arrangement of **CCl_4** molecules along the *b*-axis.

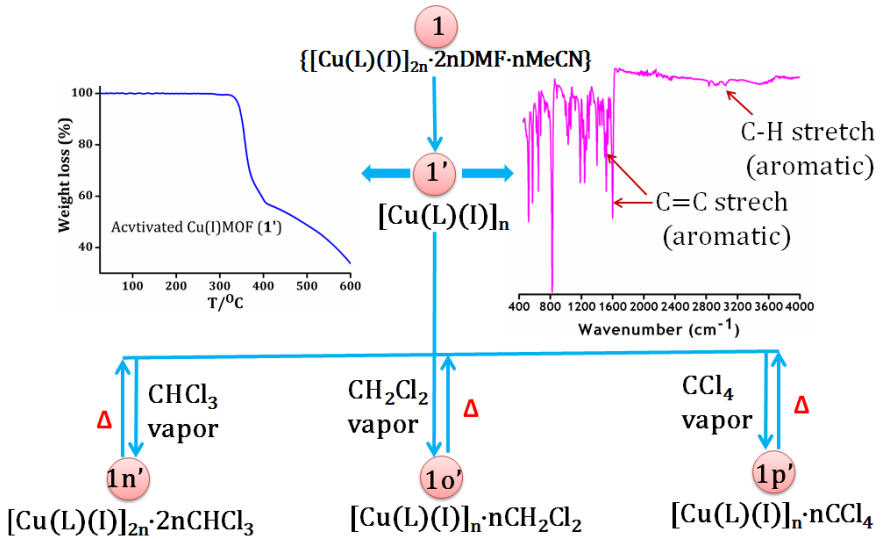

Scheme S1. Conversion of **1** to solvent free framework (**1'**) and reversible adsorption and desorption of volatile organic solvents.

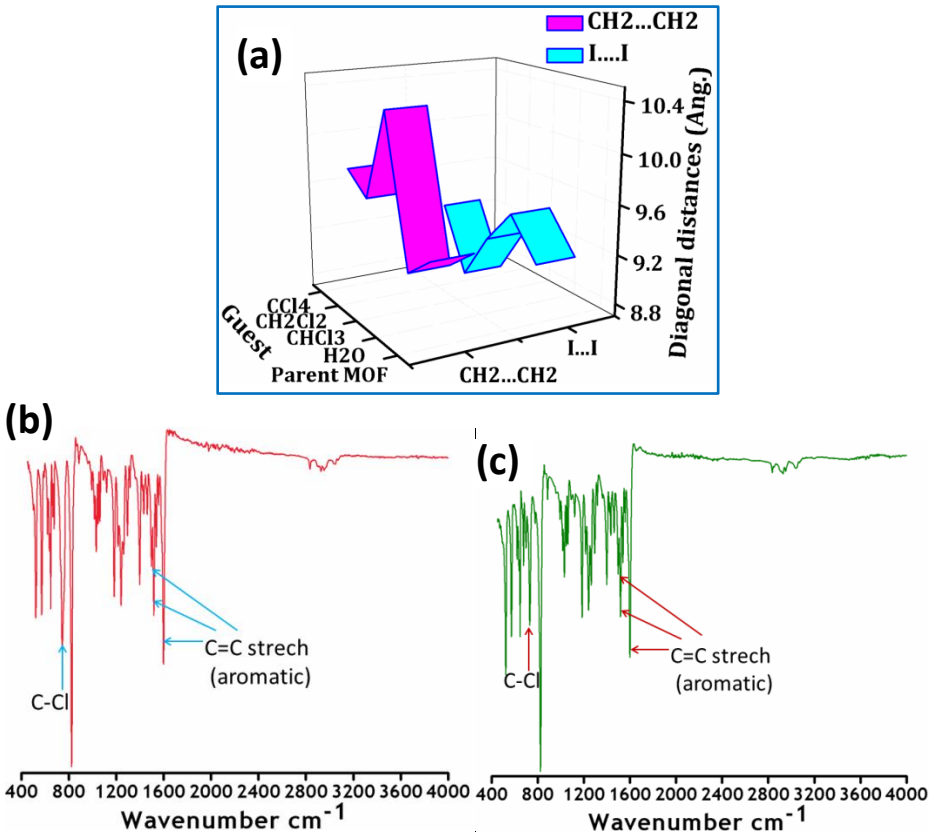

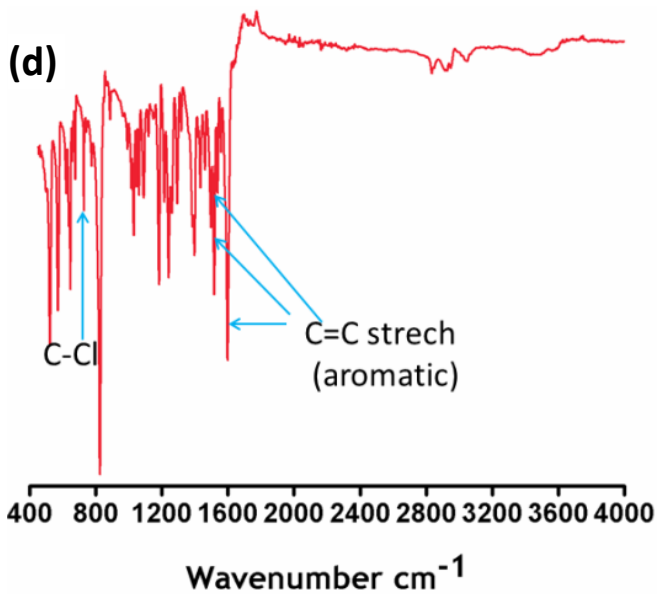

During reversible encapsulation and exclusion of the volatile solvent molecules, PXRD pattern changes. This might be due to mechanical sliding of the intertwined 2D frameworks (Figure S12d) leading to breathing behavior of the framework of Cu(I)MOF (**1**).

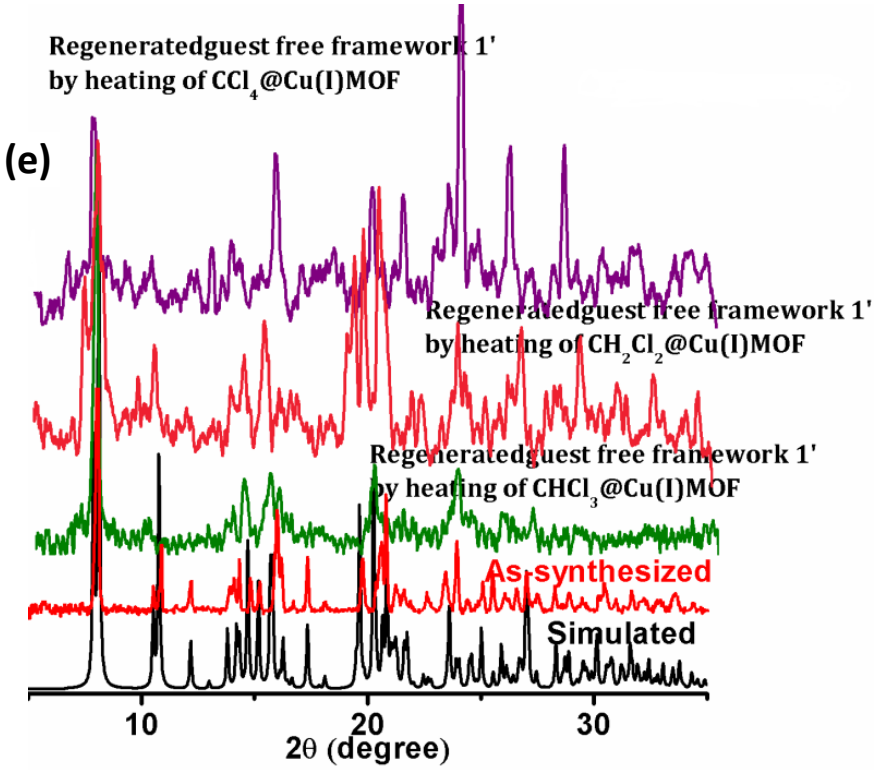

Figure S12. (a): Variation of pore dimension of **1** upon inclusion of DCE, DBE and glycol; (b-d): IR spectra of **1n'**, **1o'** and **1p'** obtained from **1'**; (e): PXRD of the regenerated guest free framework of **1'** by heating the volatile solvent included Cu(I)MOF.

Table S5. Variation of pore dimension upon inclusion of the guest molecules in 1D nanopore of the parent MOF (**1**).

Incorporated guest in Cu(I)MOF	CH2-CH2 (Å)	I2-I2 (Å)
DMF, MeCN (Parent MOF)	9.358	9.179
H_2O	9.157	9.479
$CHCl_3$	10.369	8.954
CH_2Cl_2	9.557	8.767
CCl_4	9.720	9.276
1,2-dichloro ethane (DCE)	9.641	8.811
1,2-dibromo ethane (DBE)	9.490	9.073
Ehylene glycol (glycol)	9.600	8.503
Benzene (Ph-H)	9.164	9.674
Toluene (Ph-CH_3)	9.027	9.470
1,2-dichlorobenzene (*o*-$PhCl_2$)	9.124	9.535
Aniline ($PhNH_2$)	10.371	9.466
Benzylamine ($PhCH_2NH_2$)	9.215	9.455
Naphthalene (naphtha), MeCN	8.944	9.734

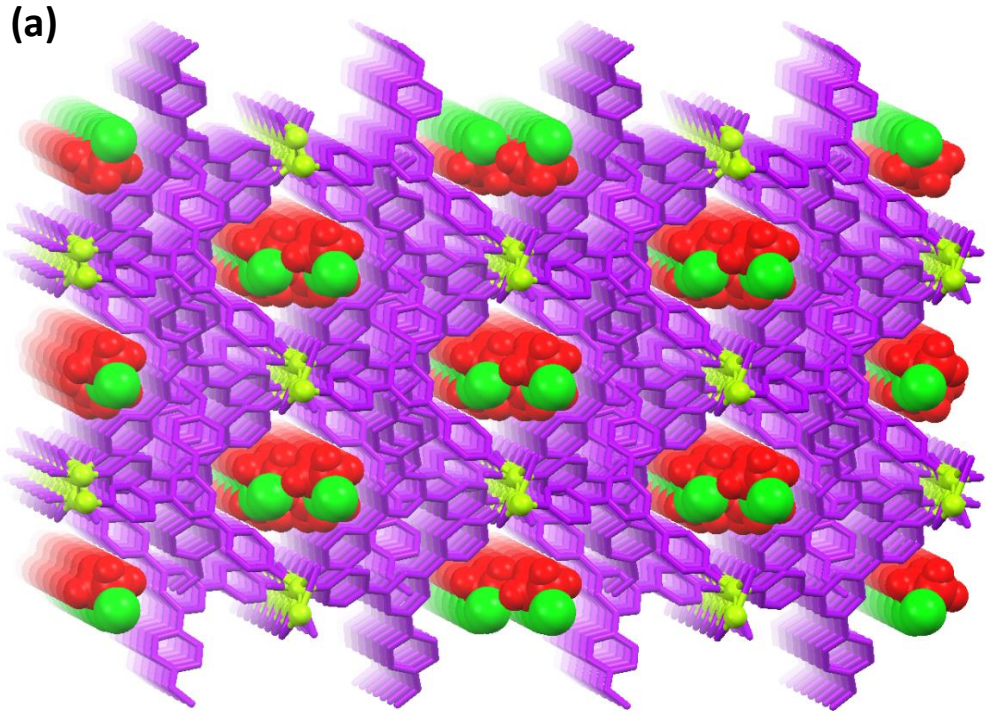

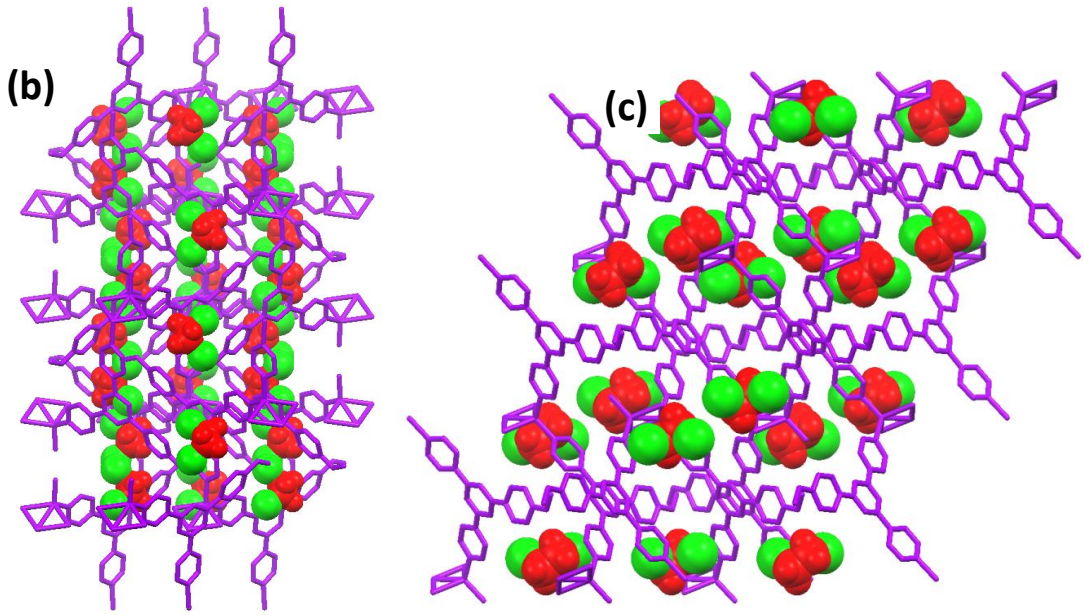

Figure S13. Solid state packing diagram of **DCE** molecules in **DCE@Cu(I)MOF** (a) down the *c-axis*; (b)-(c) zigzag arrangement of **DCE** molecules along the *a* and *b*-axes.

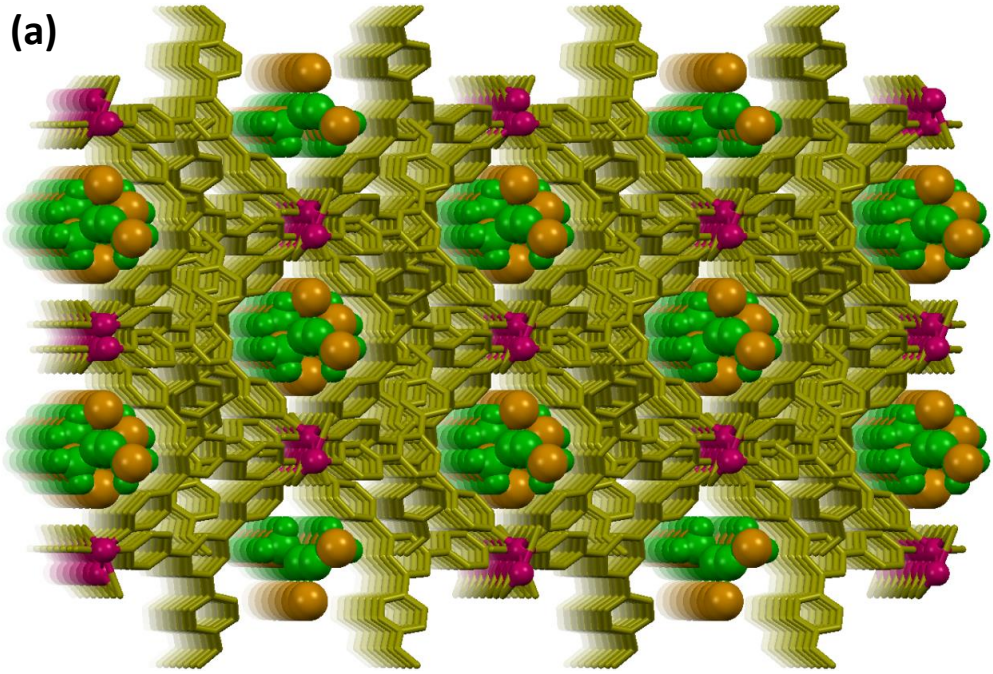

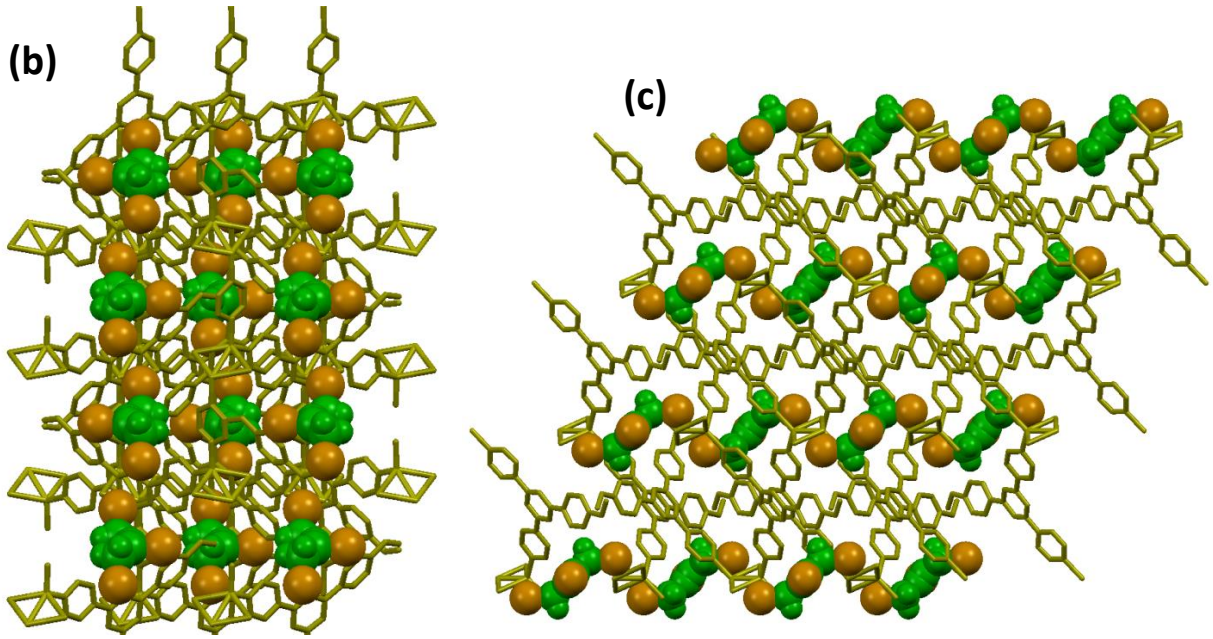

Figure 14. Solid state packing diagram of **DBE** molecules in **DBE@Cu(I)MOF** (a) down the *c-axis*; (b)-(c) zigzag arrangement of **DBE** molecules along the *a* and *b*-axes.

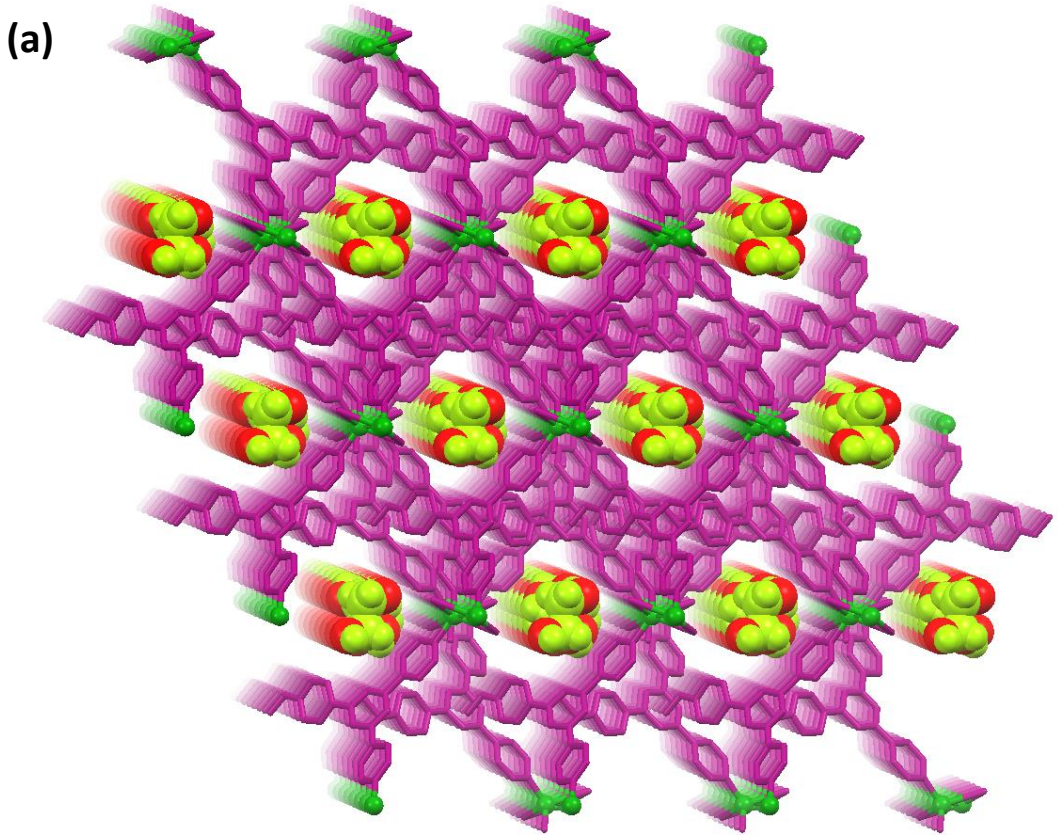

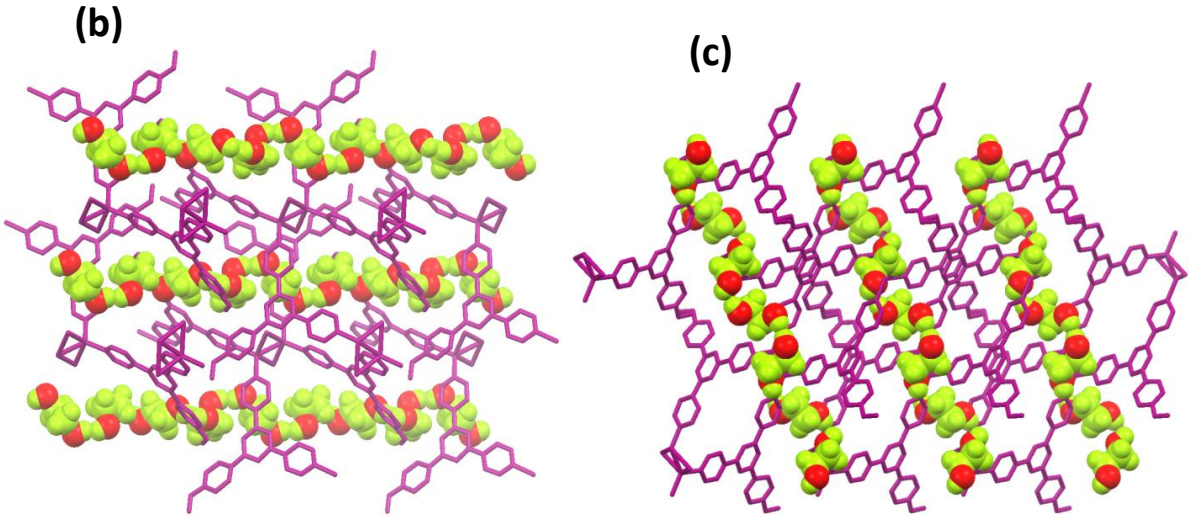

Figure 15. Solid state packing diagram of **glycol** molecules in **glycol@Cu(I)MOF** (a) down the *a-axis*; (b)-(c) zigzag arrangement of **glycol** molecules along the *b* and *c*-axes.

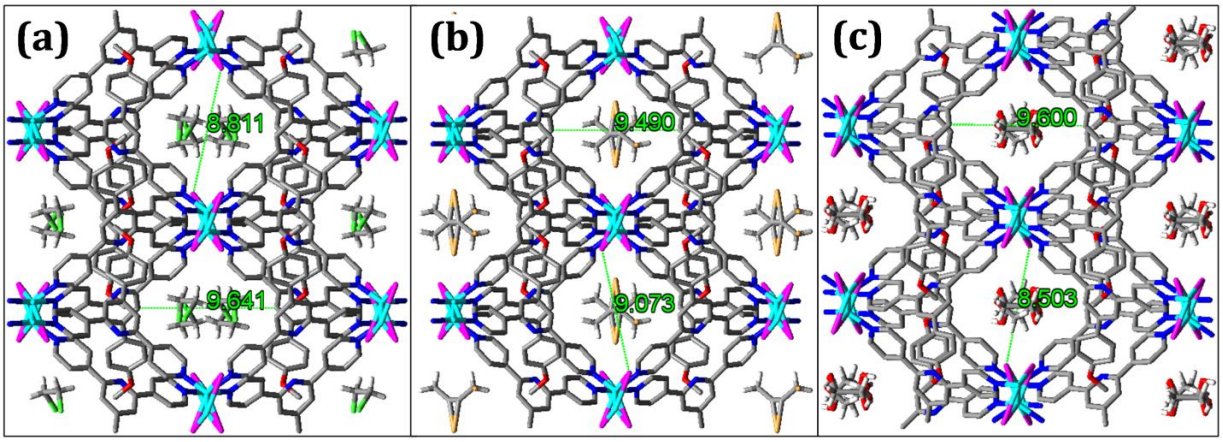

Figure S16. Change in hydrophilic length (I2⋯I2) and hydrophobic length (CH2⋯CH2) of **1** upon incorporation of different rotational isomers (a) DCE (b) DBE (c) glycol.

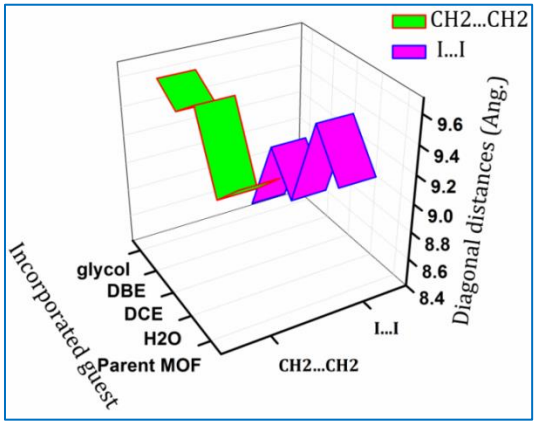

Figure S17. Variation of pore dimension of **1** upon inclusion of DCE, DBE and glycol.

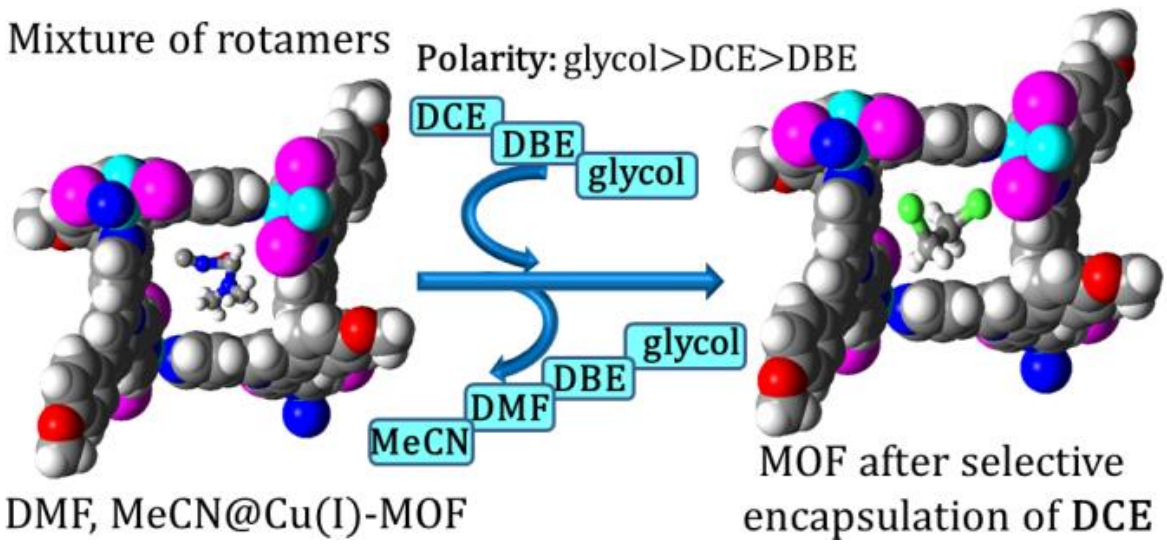

Scheme S2. Schematic Representation of the Selective Incorporation of DCE among Various Rotamers.

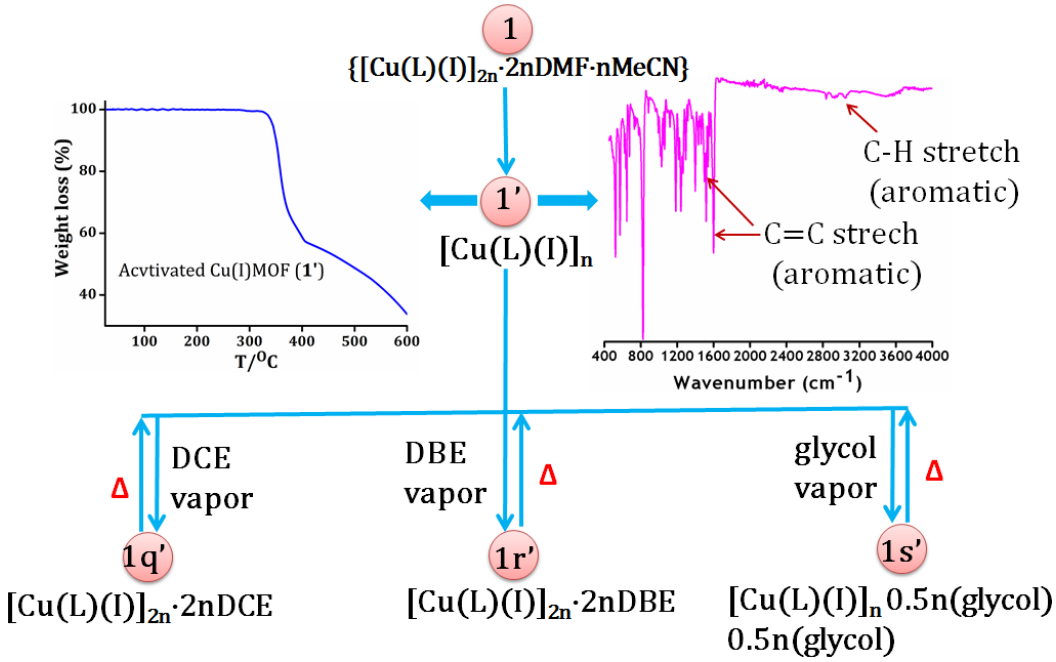

Scheme S3. Conversion of **1** to the desolvated framework (**1'**) and reversible adsorption and desorption of rotational isomers.

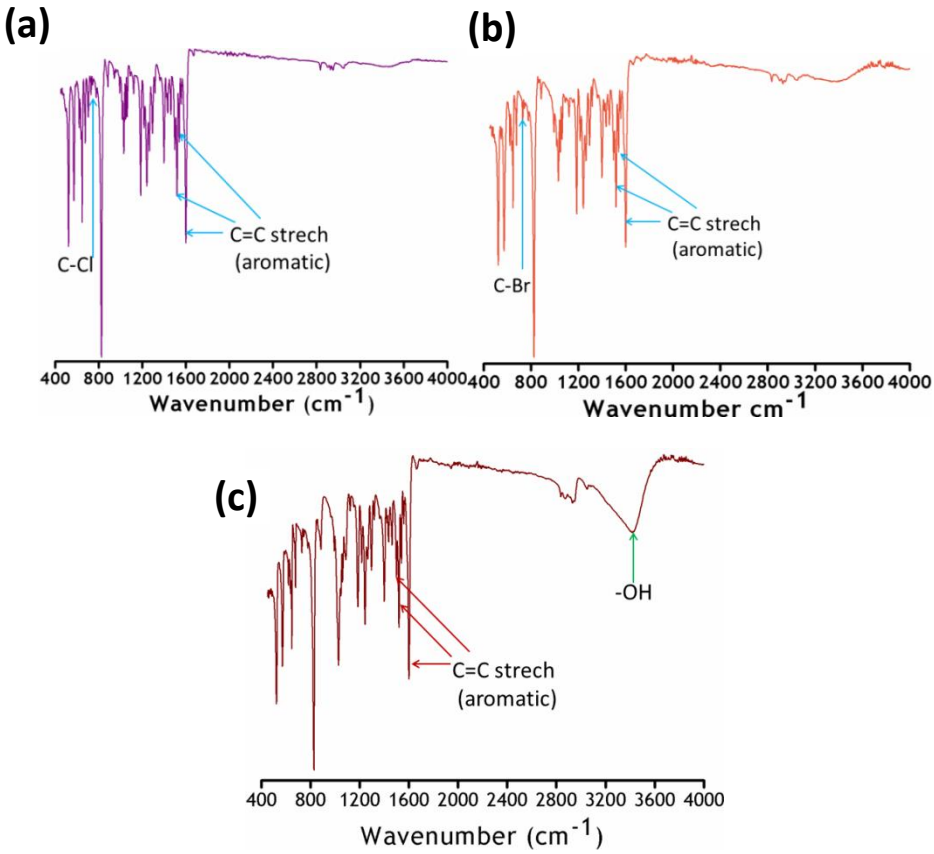

PXRD patterns change during reversible inclusion and exclusion of the rotational isomers. This can be attributed to mechanical sliding of the interpenetrated 2D frameworks (Figure S18d) leading to dynamic behavior of the framework of Cu(I)MOF.

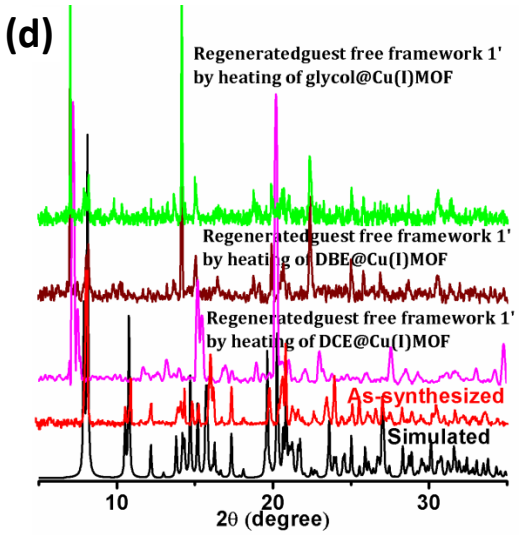

Figure S18. (a-c): IR spectra of **1q'**, **1r'** and **1s'** obtained from **1'**; (d): PXRD of the regenerated guest free framework of **1'** by heating the rotational isomers included Cu(I)MOF.

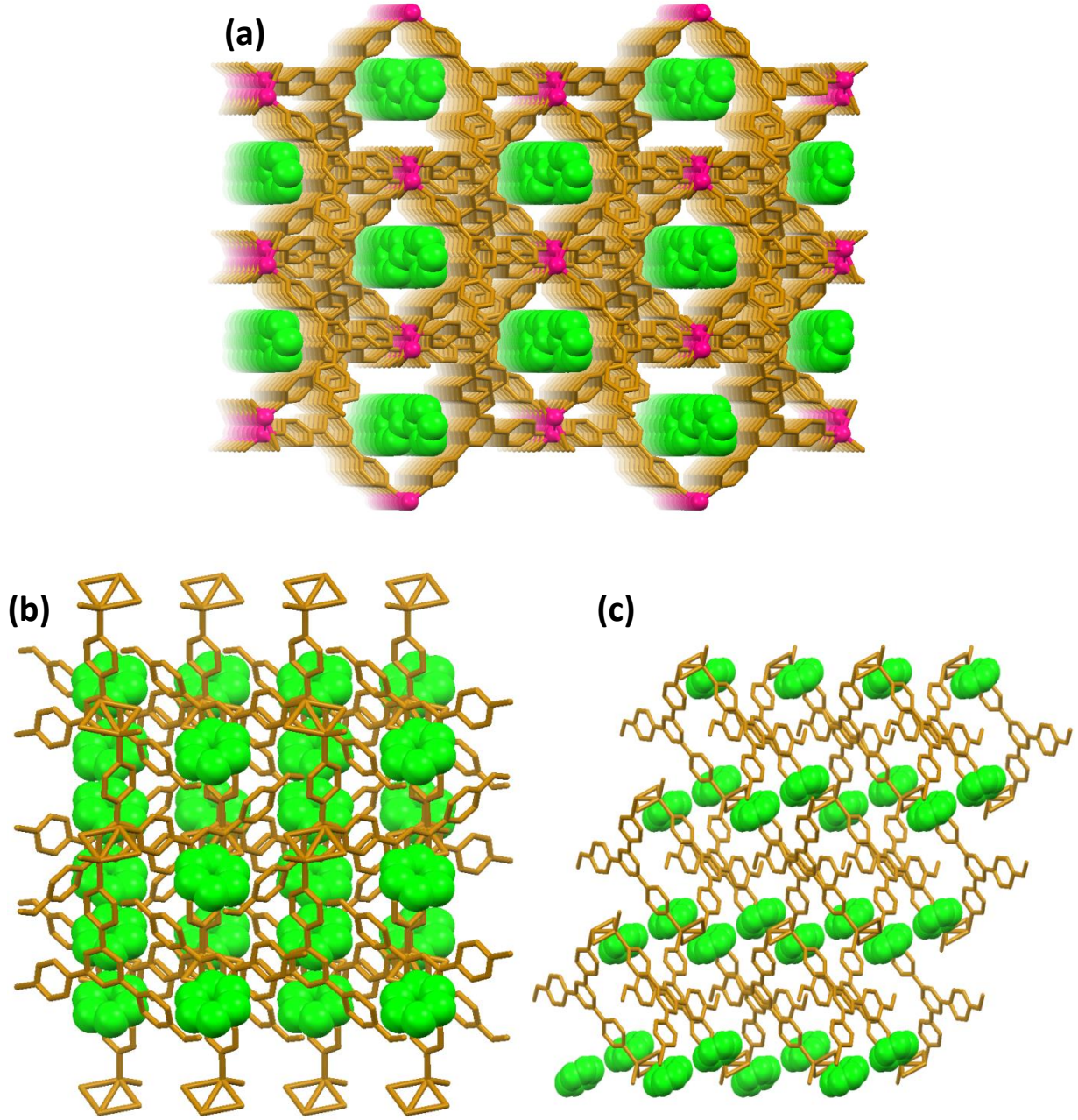

Figure S19. Solid state packing diagram of **PhH** molecules in **PhH@Cu(I)MOF** (a) down the *c-axis*; (b)-(c) zigzag arrangement of **PhH** molecules along the *a* and *b*-axes.

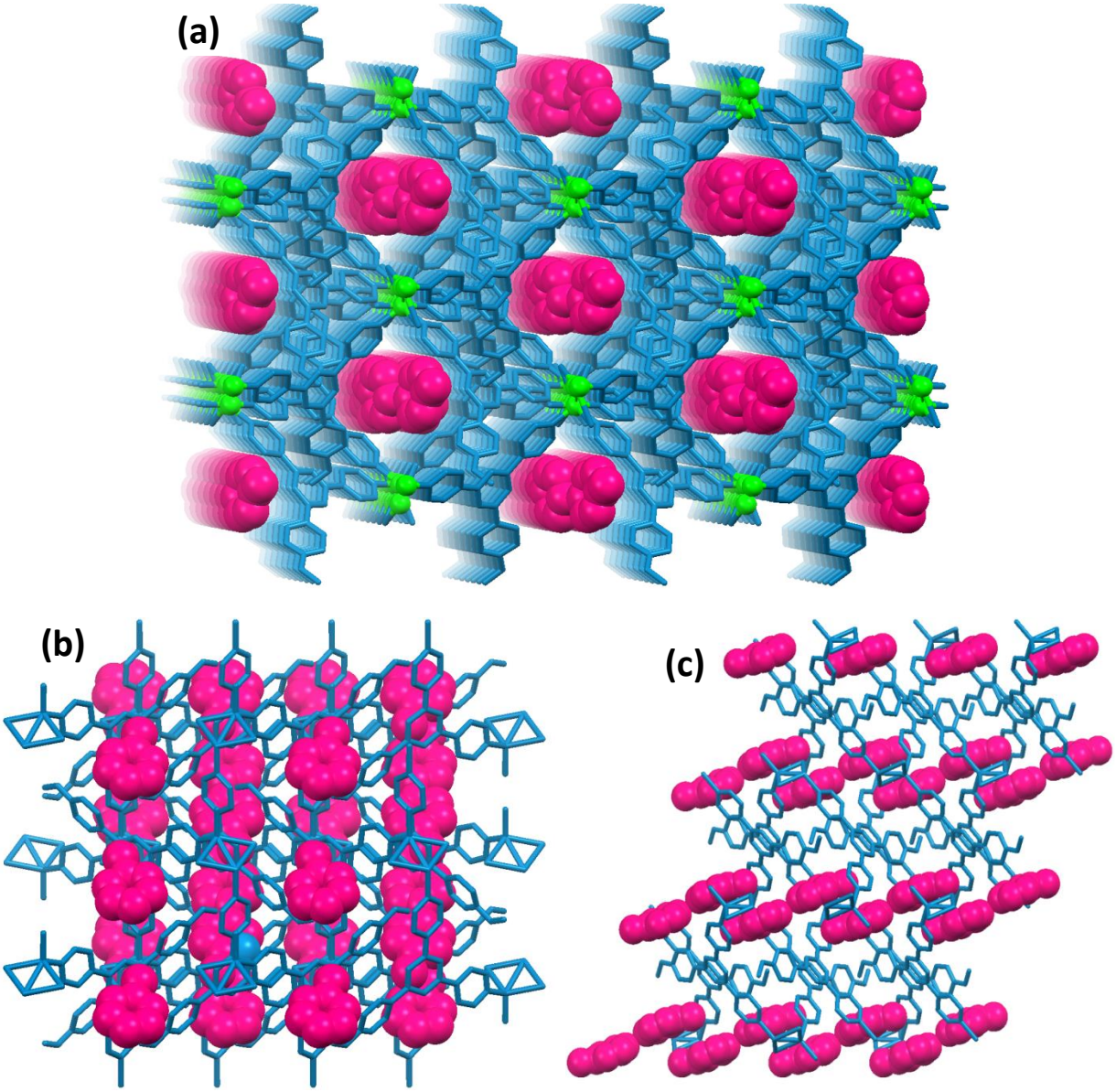

Figure S20. Solid state packing diagram of **$PhCH_3$** molecules in **$PhCH_3$@Cu(I)MOF** (a) down the *c-axis*; (b)-(c) zigzag arrangement of **$PhCH_3$** molecules along the *a* and *b*-axes.

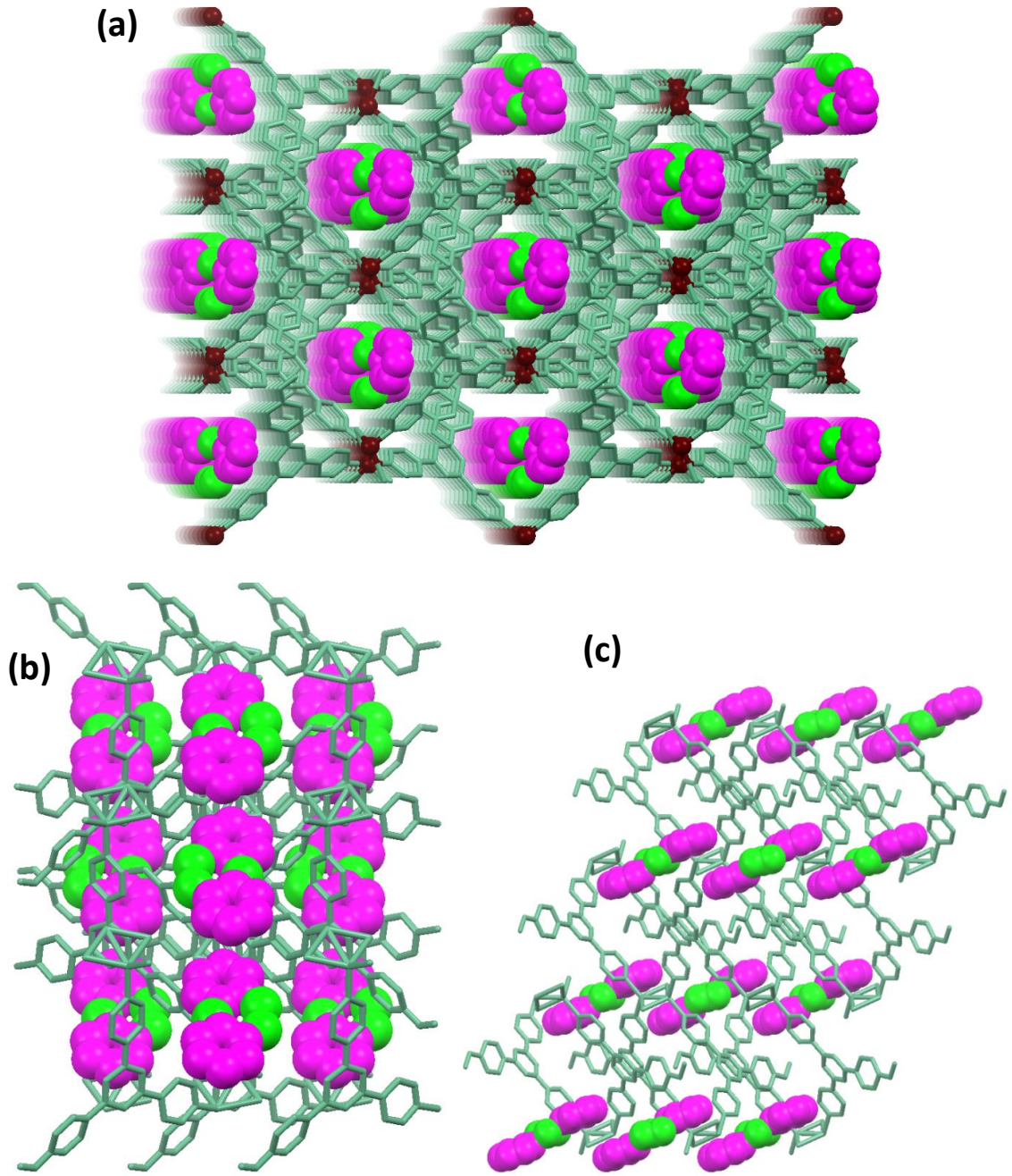

Figure S21. Solid state packing diagram of ***o*-PhCl$_2$** molecules in ***o*-PhCl$_2$@Cu(I)MOF** (a) down the *c-axis*; (b)-(c) zigzag arrangement of ***o*-PhCl$_2$** molecules along the *a* and *b*-axes.

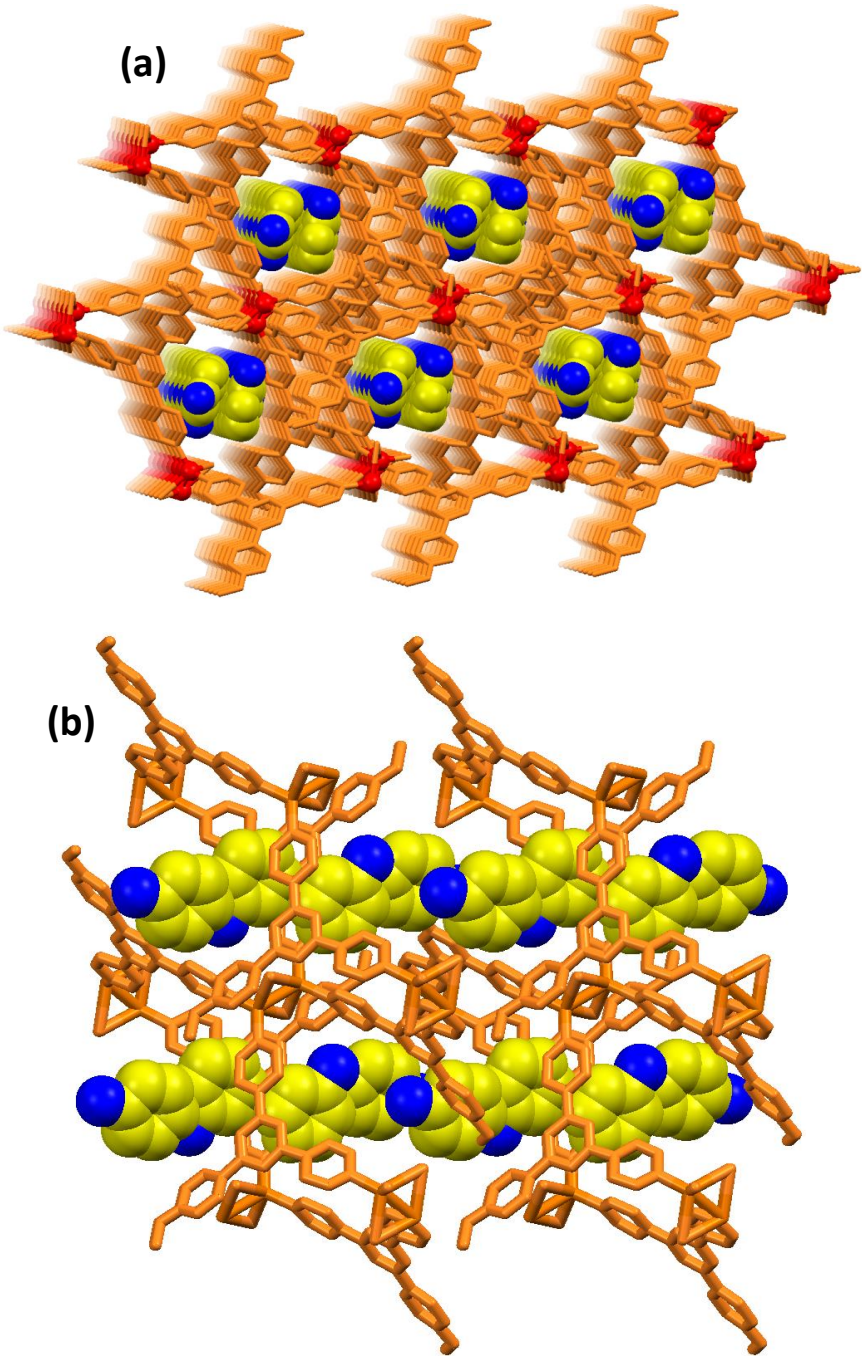

Figure S22. Solid state packing diagram of **PhNH$_2$** molecules in **PhNH$_2$@Cu(I)MOF** (**1w**) (a) down the *b-axis*; (b) zigzag arrangement of **PhNH$_2$** molecules along the *c-axis*.

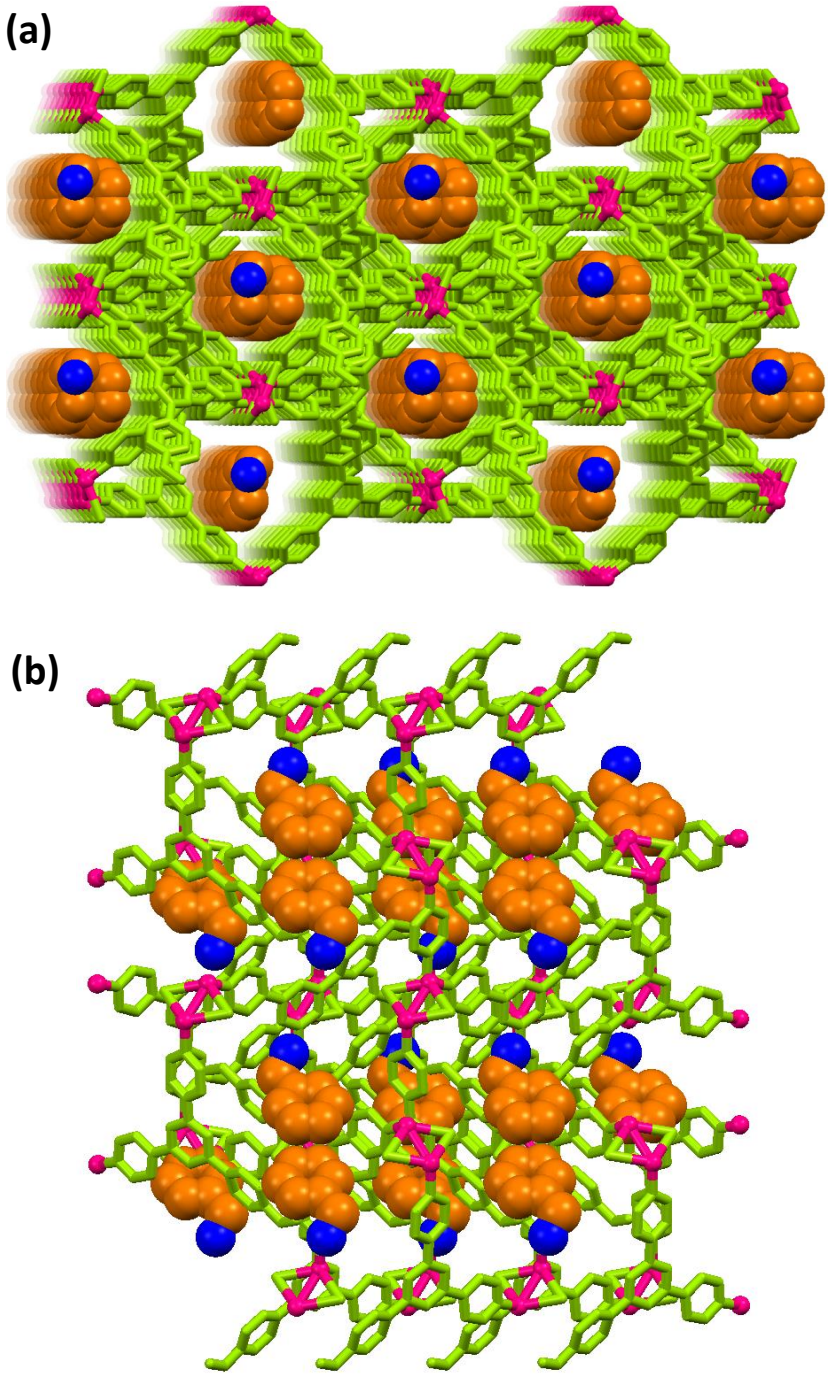

Figure S23. Solid state packing diagram of **$PhCH_2NH_2$** molecules in **$PhCH_2NH_2$@Cu(I)MOF** (**1x**) (a) down the *c-axis*; (b) zigzag arrangement of **$PhCH_2NH_2$** molecules along the *a-axis*.

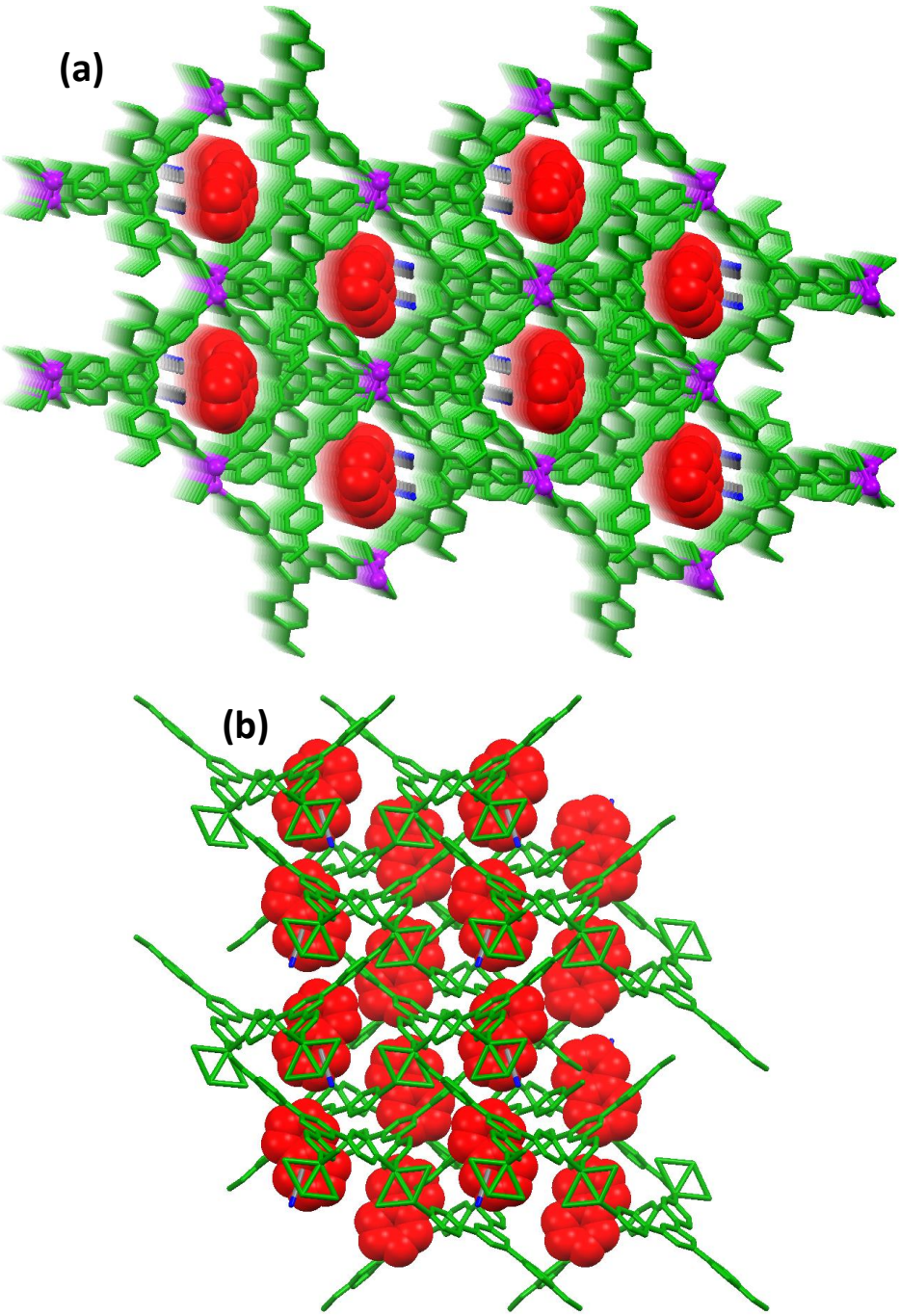

Figure S24. Solid state packing diagram of **naphthalene** molecules in **naphtha@Cu(I)MOF** (**1y**) (a) down the *c-axis*; (b) zigzag arrangement of **naphtha** molecules along the *a*-axis.

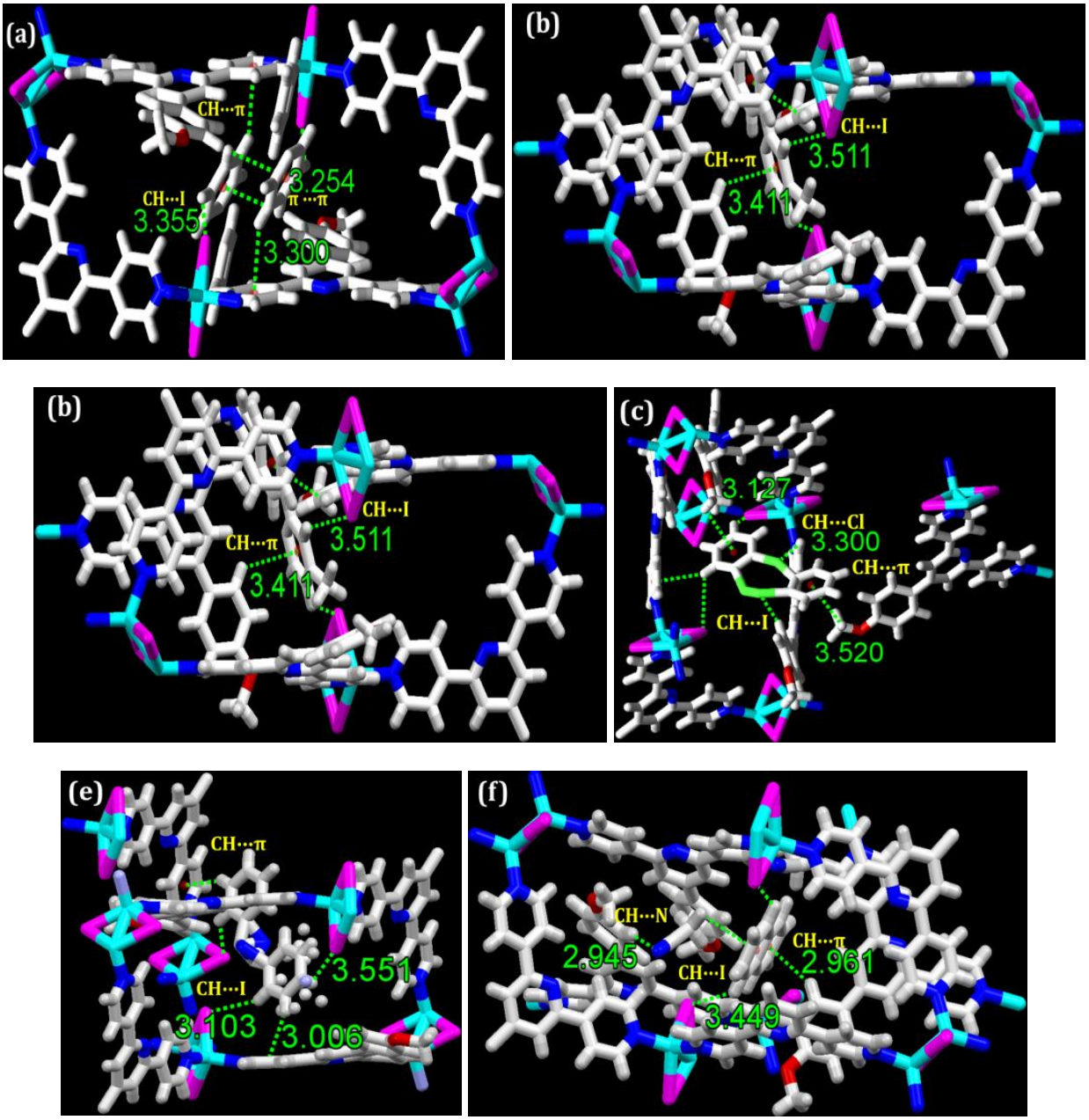

Figure S25. Non covalent interactions of the MOF with the incorporated guest molecules (a) Ph-H; (b) Ph-CH_3; (c) *o*-$PhCl_2$; (d) Ph-NH_2; (e) Ph-CH_2NH_2; (f) Naphtha.

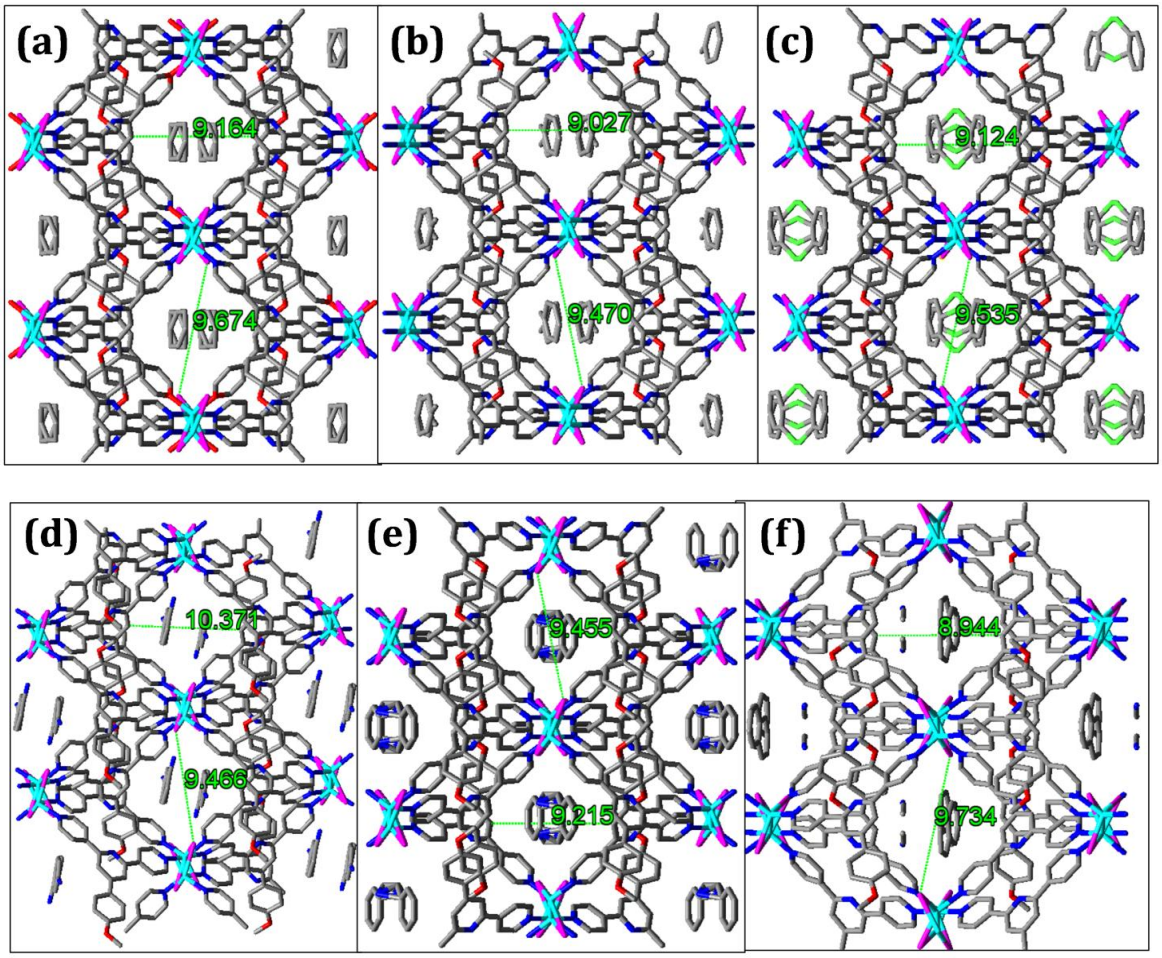

Figure S26. Change in hydrophilic length (I2⋯I2) and hydrophobic length (CH2⋯CH2) upon incorporation of benzene and its derivatives and naphthalene (a) benzene (b) toluene (c) o-$PhCl_2$ (d) $PhNH_2$ (e) $PhCH_2NH_2$ (f) Naphtha.

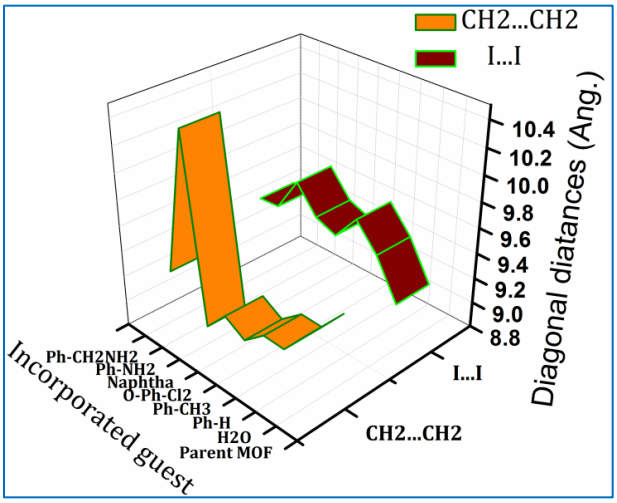

Figure S27. Variation of pore dimension of **1** upon inclusion of benzene and its derivatives and naphthalene.

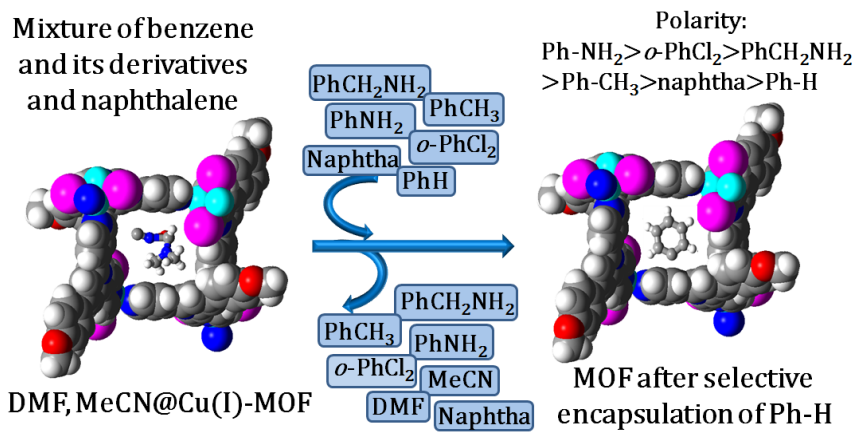

Scheme S4. Schematic representation of the selective incorporation of benzene among benzene and its derivatives, and naphthalene.

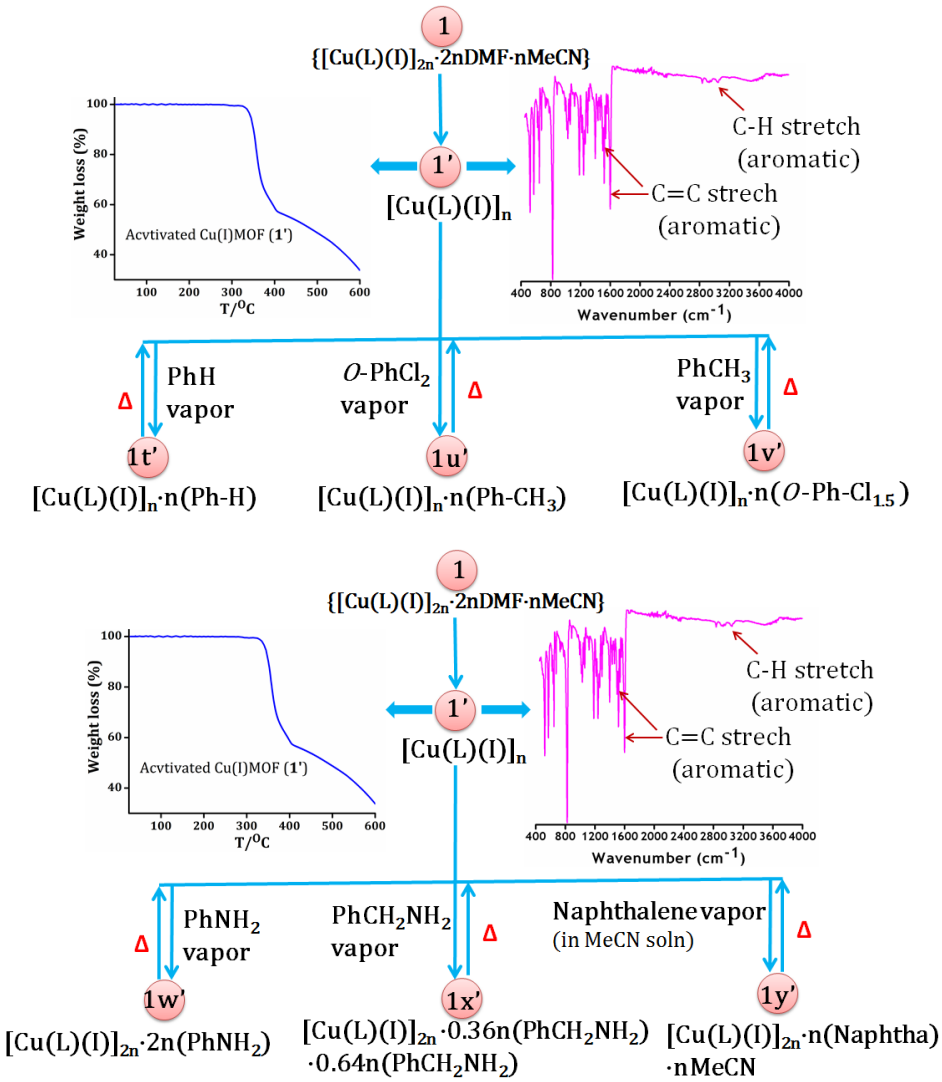

Scheme S5. Conversion of **1** to the desolvated framework (**1'**) and reversible adsorption and desorption of benzene and its derivatives, and naphthalene.

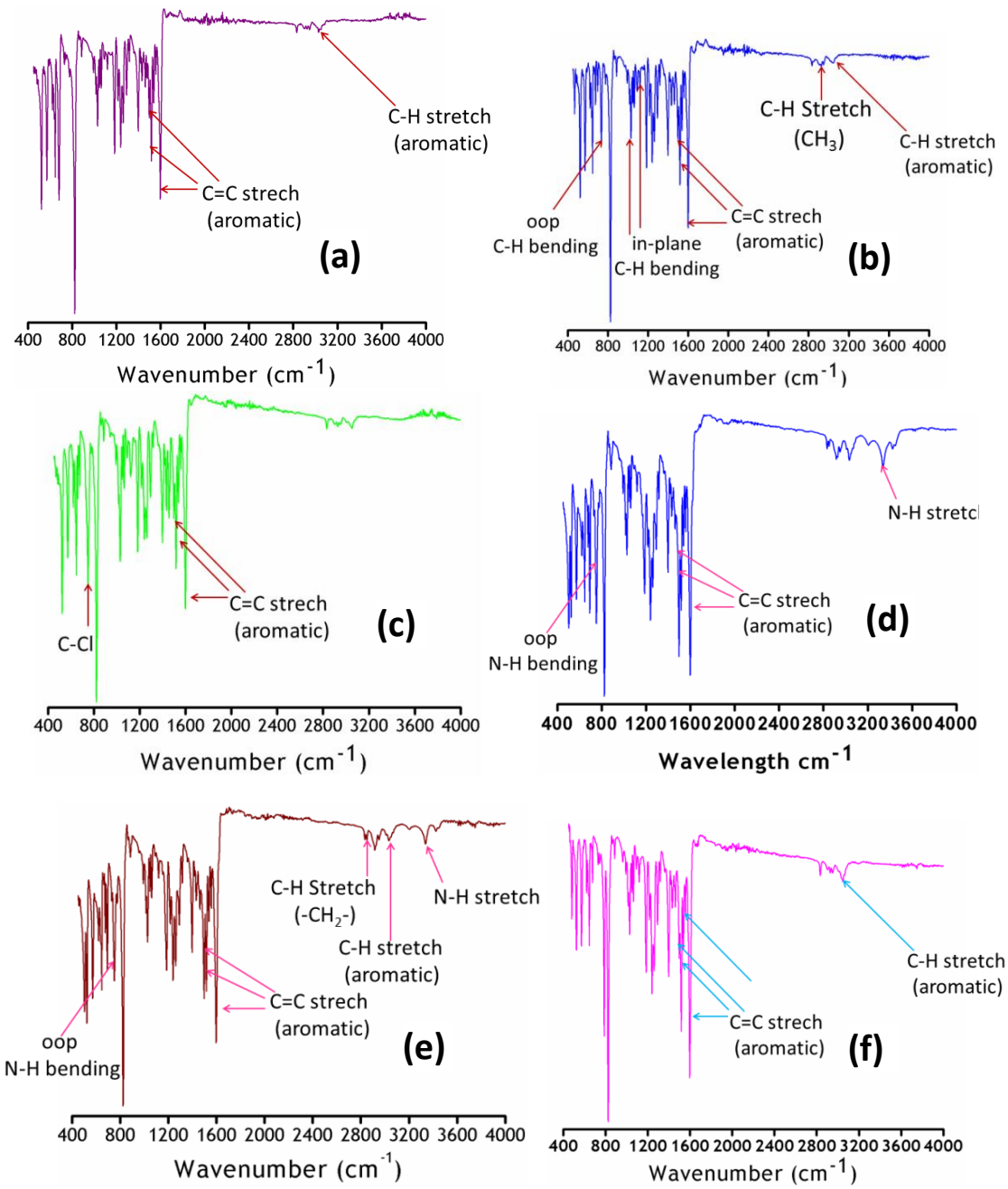
C-H stretch
(aromatic)
C=C strech
(aromatic)
(a)
400 800 1200 1600 2000 2400 2800 3200 3600 4000
Wavenumber (cm-1)
C-H Stretch
(CH3)
C-H stretch
(aromatic)
oop
C-H bending
in-plane
C-H bending
C=C strech
(aromatic)
(b)
400 800 1200 1600 2000 2400 2800 3200 3600 4000
Wavenumber (cm-1)
C-Cl
C=C strech
(aromatic)
(c)
400 800 1200 1600 2000 2400 2800 3200 3600 4000
Wavenumber (cm-1)
N-H stretc
C=C strech
(aromatic)
oop
N-H bending
(d)
400 800 1200 1600 2000 2400 2800 3200 3600 4000
Wavelength cm-1
C-H Stretch
(-CH2-)
N-H stretch
C-H stretch
(aromatic)
C=C strech
(aromatic)
oop
N-H bending
(e)
400 800 1200 1600 2000 2400 2800 3200 3600 4000
Wavenumber (cm-1)
C-H stretch
(aromatic)
C=C strech
(aromatic)
(f)
400 800 1200 1600 2000 2400 2800 3200 3600 4000
Wavenumber (cm-1)

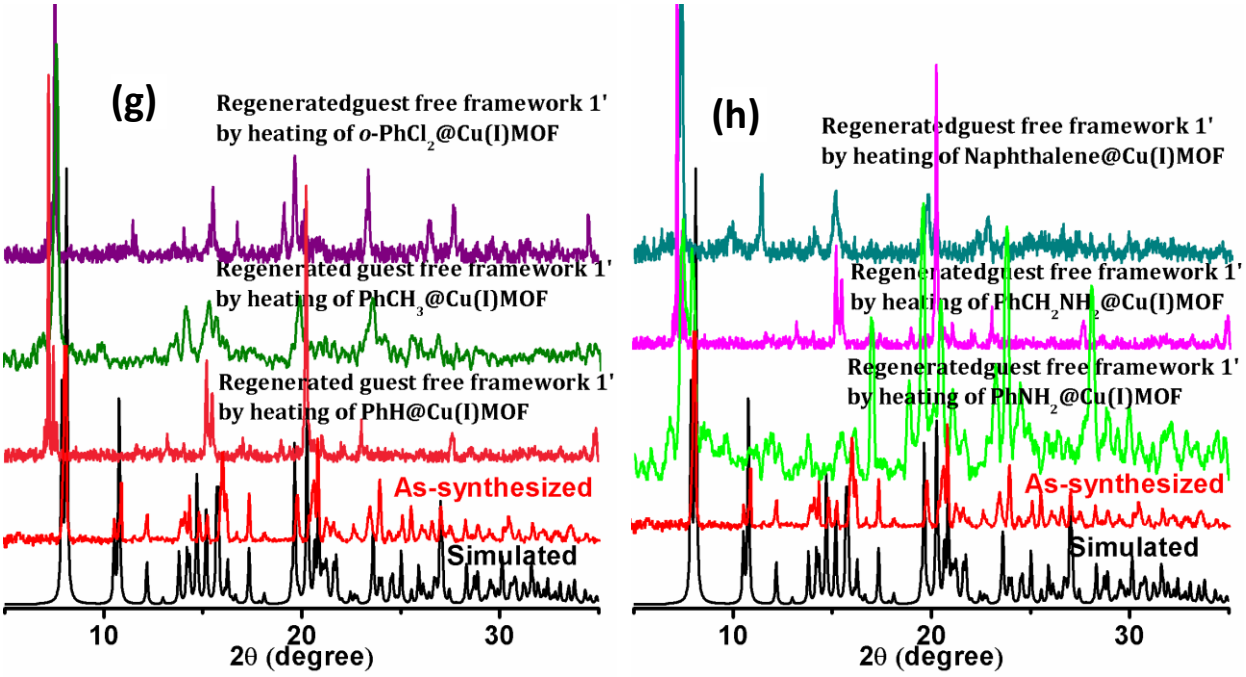

Figure S28. (a-f) IR spectra of **1t'**, **1u'**, **1v', 1w', 1x'** and **1y'** obtained from **1'**; (g-h): PXRD of the regenerated guest free framework of **1'** by heating the benzene and its derivative and naphthalene included Cu(I)MOF.

PXRD analysis reveals that the pattern changes during reversible inclusion and exclusion of the benzene and its derivatives and naphthalene. This can be attributed to mechanical sliding of the intertwined 2D frameworks (Figure S28g-h and Figures S29-S32) illustrating dynamic behavior of the framework of Cu(I)MOF.

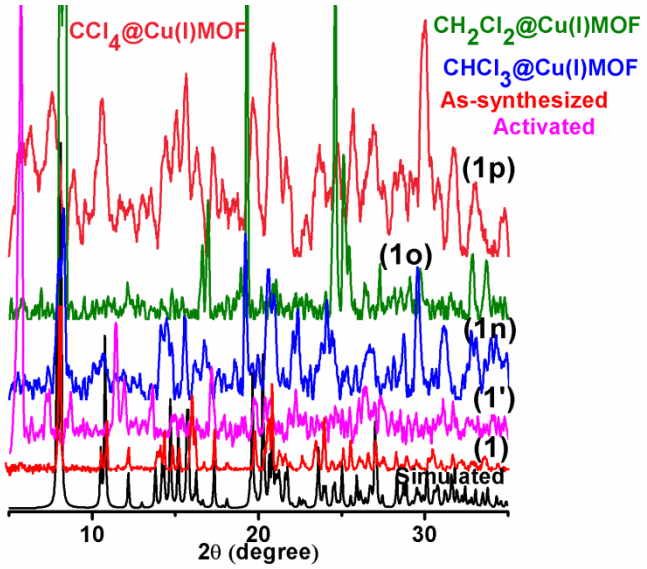

Figure S29. RT PXRD patterns reveal the breathing behavior of activated (**1'**) and guest exchanged complexes (**1n**, **1o** and **1p**) by gentle grinding showing phase transformation.

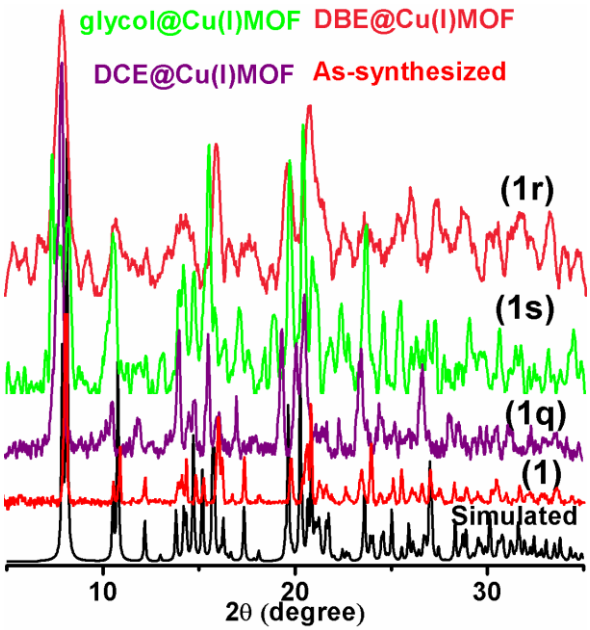

Figure S30. RT PXRD patterns reveal the breathing behavior of guest exchanged complexes (**1q**, **1r** and **1s**) by gentle grinding showing phase transformation.

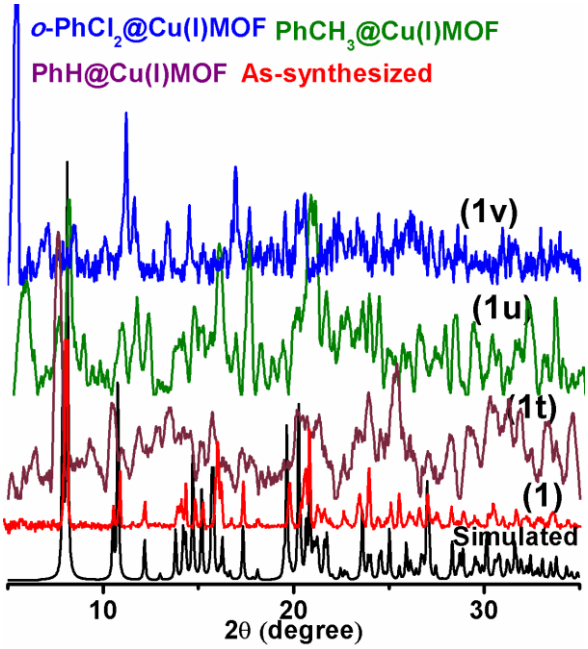

Figure S31. RT PXRD patterns reveal the breathing behavior of guest exchanged complexes (**1t**, **1u** and **1v**) by gentle grinding showing phase transformation.

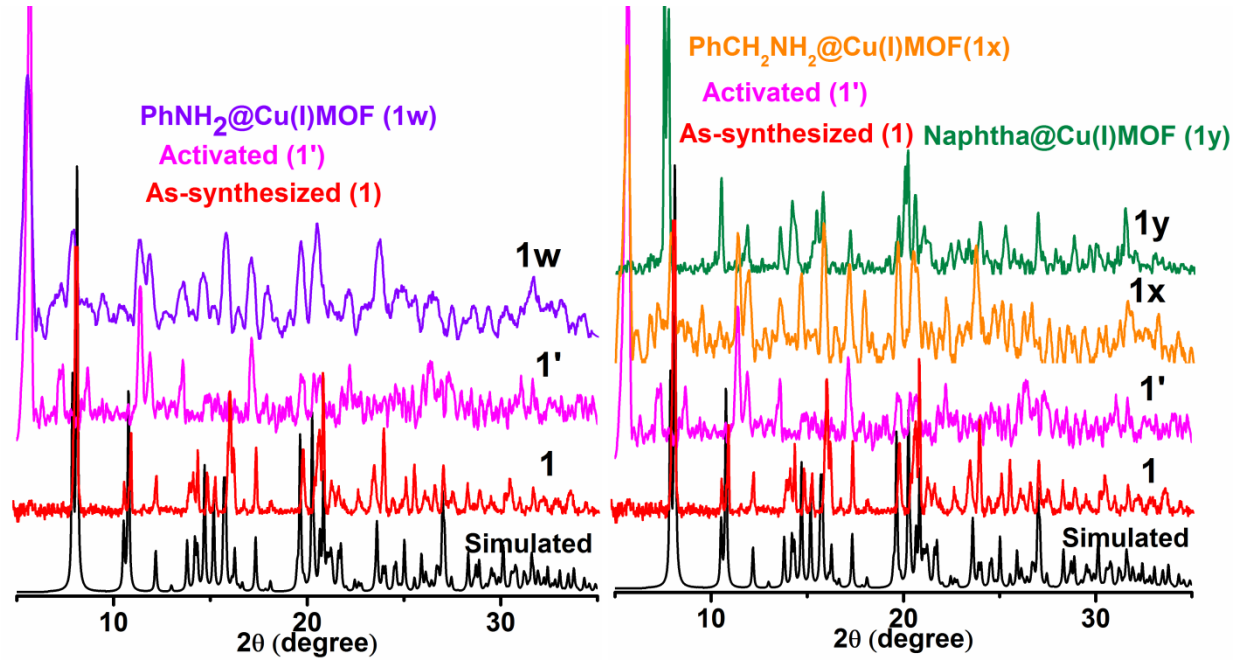

Figure S32. RT PXRD patterns reveal the breathing behavior of activated (**1'**) and guest exchanged complexes (**1w**, **1x** and **1y**) by gentle grinding showing phase transformation.

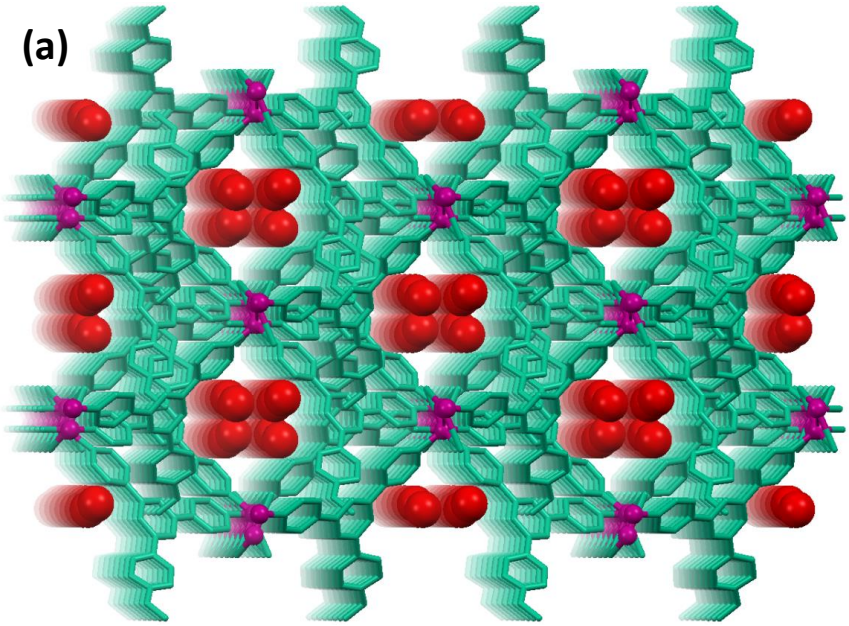

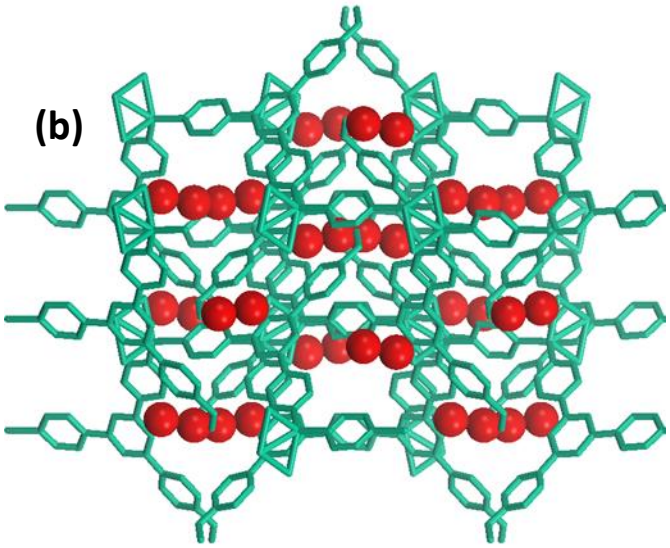

Figure S33. Solid state packing diagram of **H_2O** molecules in **H_2O@Cu(I)MOF** (as **intermediate** prior to guest inclusion) (a) down the *c-axis*; (b) zigzag arrangement of **H_2O** molecules along the *a-axis*.

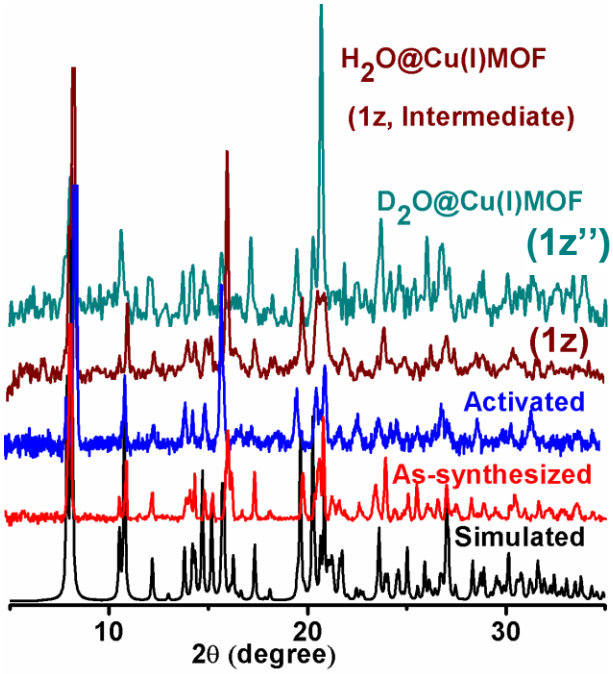

Figure S34. PXRD patterns of the simulated, as-synthesized (**1**), activated (**1'**), intermediate (**H_2O@Cu(I)MOF**) and **D_2O@Cu(I)MOF** included complexes.

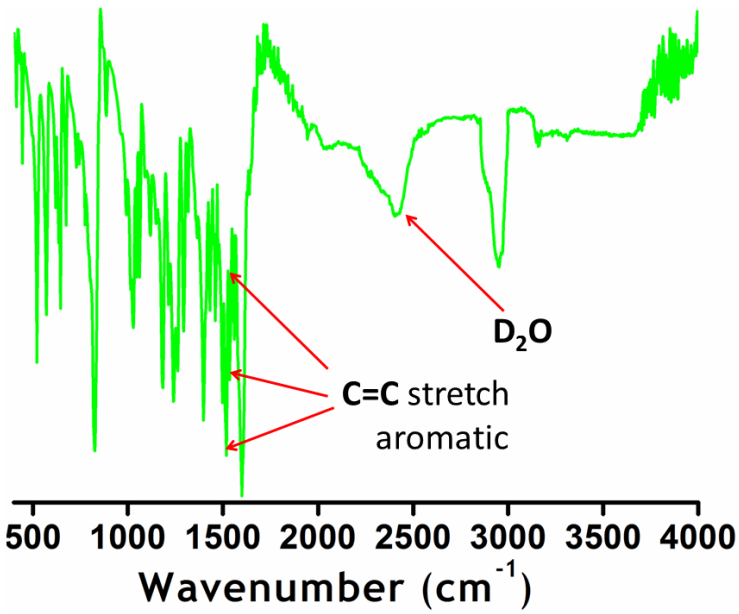

Figure S35. FTIR of **D_2O@Cu(I)MOF** in the presence of other guests.

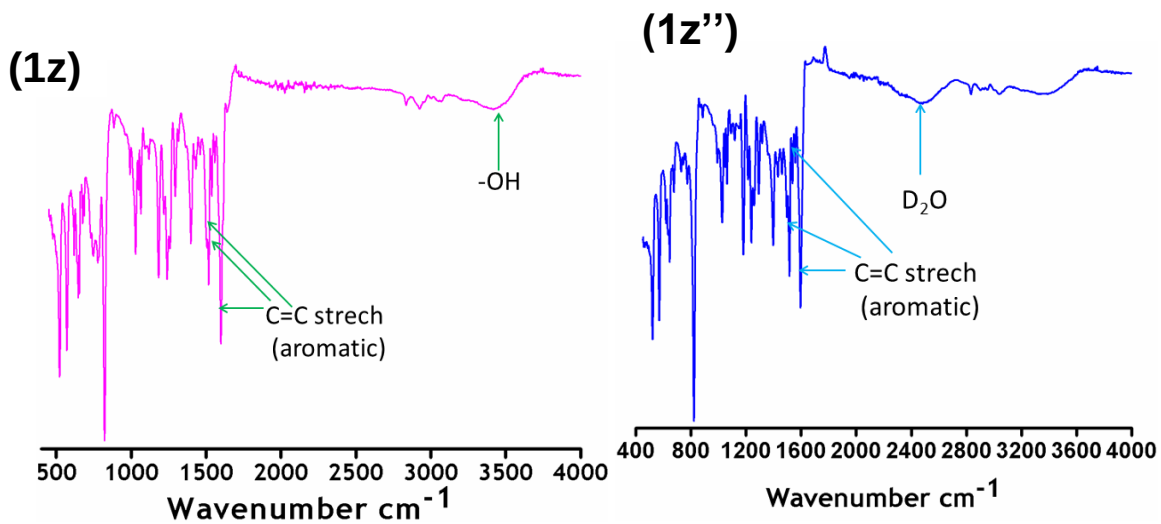

Figure S36. FTIR of **H_2O@Cu(I)MOF** (**1z**) and **D_2O@Cu(I)MOF** (**1z''**).

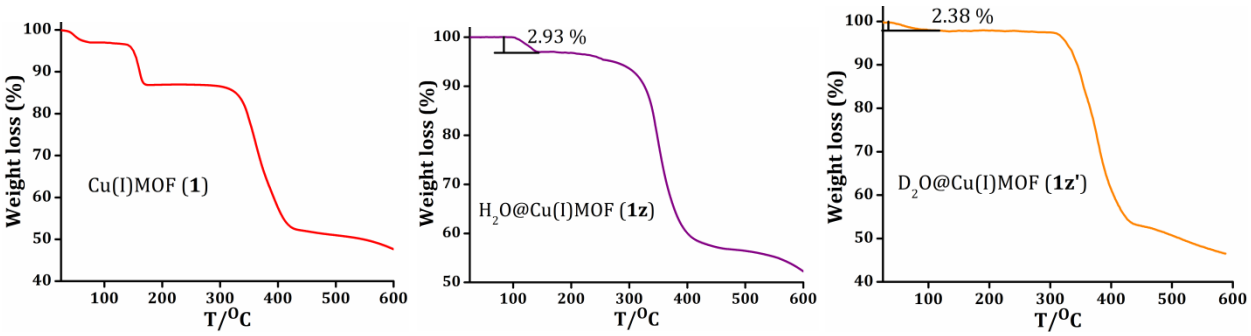

Figure S37. TGA thermograms of **1**, **H_2O@Cu(I)MOF** (**1z**) and **D_2O@Cu(I)MOF** (**1z''**).

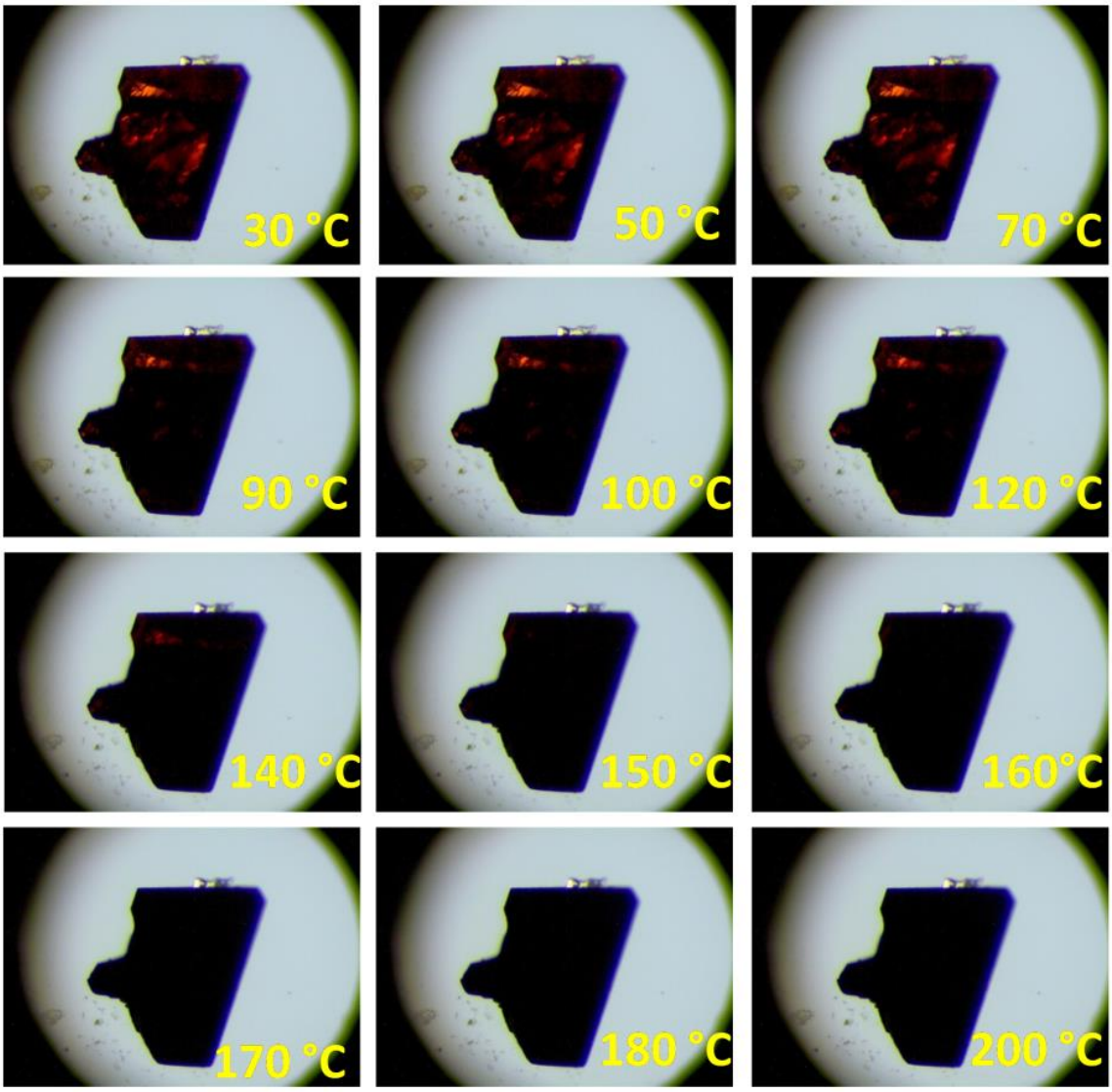

Figure S38. Hot stage microscopic image of the parent MOF (**1**) taken at different temperature.

Guest responsive geometry change of parent MOF: For the guest molecules such as **CH_2Cl_2**, **CCl_4**, **DCE**, **DBE**, **glycol**, **PhH**, **$PhCH_3$**, ***o*-$PhCl_2$**, and **$PhCH_2NH_2$** in **1o**, **1p**, **1q**, **1r**, **1s**, **1t**, **1u**, **1v**, and **1x** are crystallized in monoclinic system, Rhombohedral geometry remains the same as found in the parent MOF (**1**) and the intermediate (**1z**). But, for **naphthalene** in **1y** also crystalizes in the same system with different space group no specific geometry is observed. For the guest molecule **$CHCl_3$** and **$PhNH_2$** in **1n** and **1w**, respectively, are crystallized in triclinic system, the rhombohedral geometry is changed into parallelogram. Thus, we can say that upon inclusion of the guest molecules, geometry of the parent MOF is changed which signifies its dynamic and flexible behavior (Figures S39-S41).

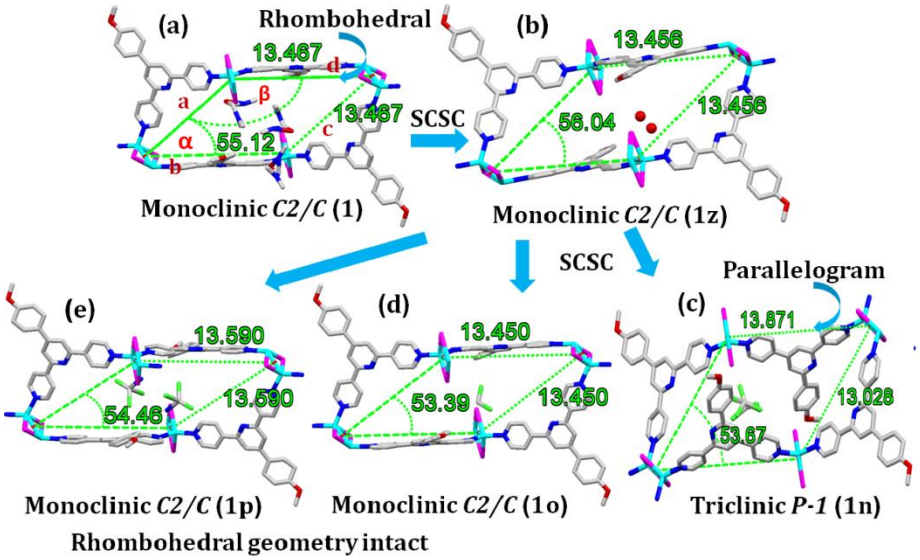

Figure S39. Variation of edge lengths and angles of rhombohedral geometry of the parent MOF (**1**) upon inclusion of different volatile organic solvents (a) parent MOF; (b) water in **1z**; **(**c) $CHCl_3$ in **1n**; (d) CH_2Cl_2 in **1o**; (e) **CCl_4** in **1p**.

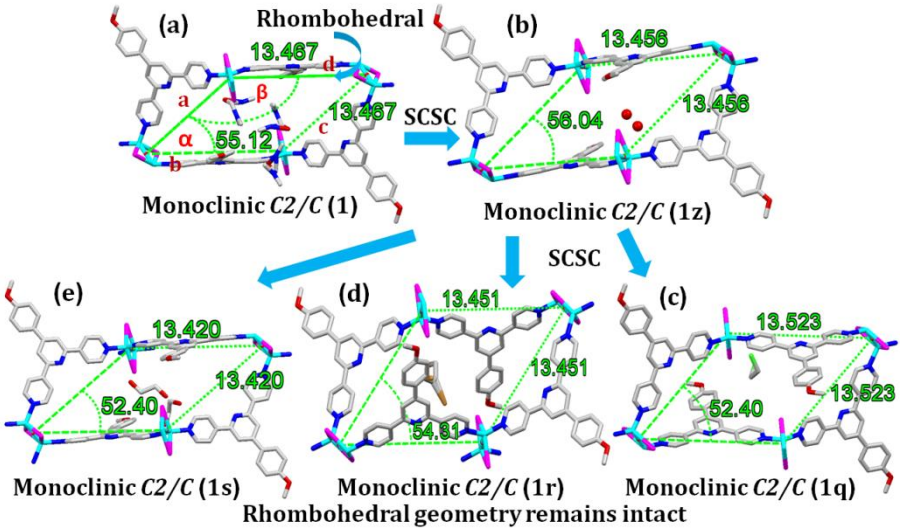

Figure S40. Variation of edge lengths and angles of rhombohedral geometry of the parent MOF (**1**) upon inclusion of different rotational isomers (a) parent MOF; (b) water in **1z**; **(**c) DCE in **1q**; (d) DBE in **1r**; (e) glycol in **1s**.

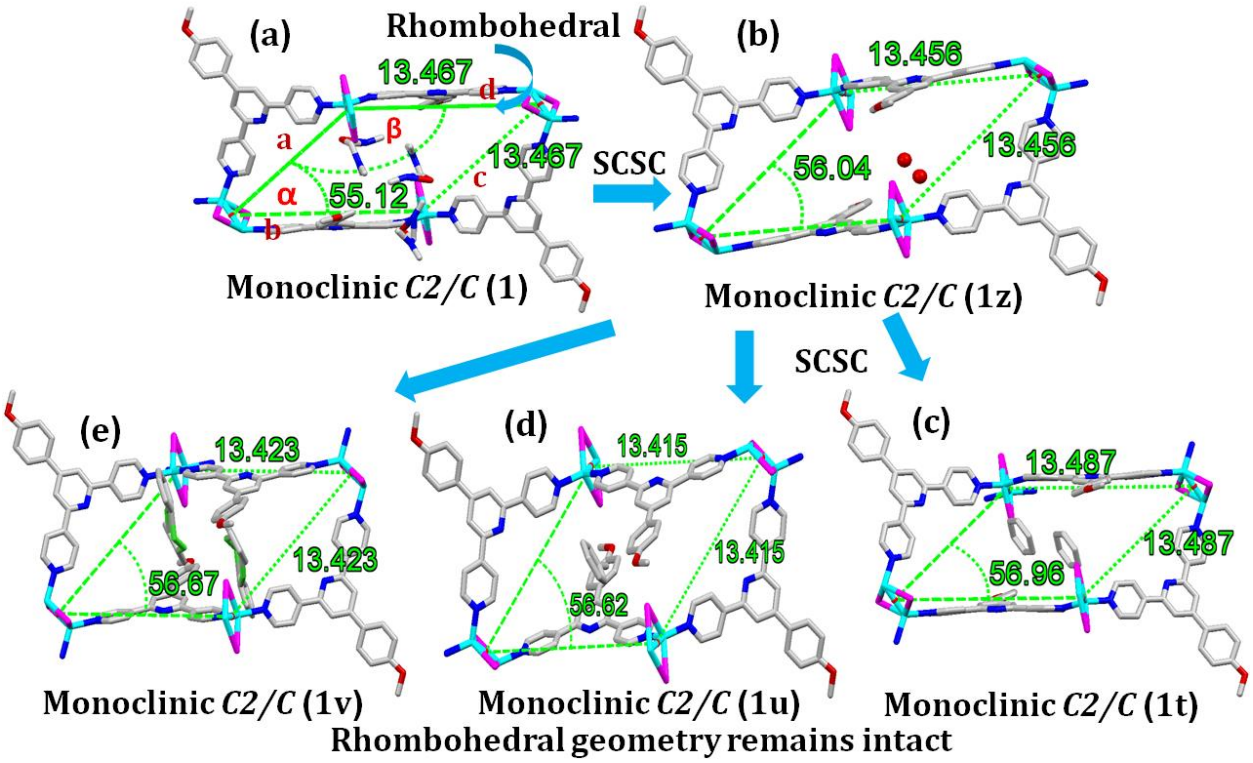

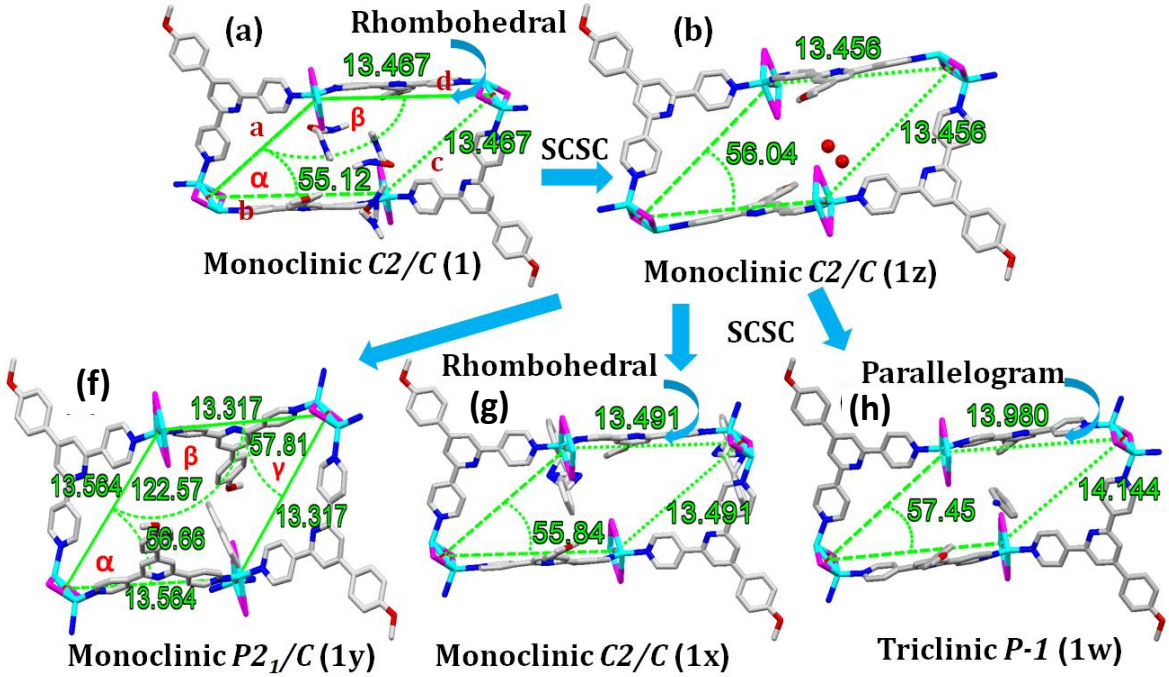

Figure S41. Variation of edge lengths and angles of rhombohedral geometry of the parent MOF (**1**) upon inclusion of benzene and its derivatives and naphthalene (a) parent MOF; (b) H_2O in **1z**; **(**c) Benzene in **1t**; (d) Toluene in **1u**; (e) o-$PhCl_2$ in **1v**; (f) Naphthalene in**1y**; (g) $PhCHNH_2$ in **1x**; (h) $PhNH_2$ in **1w**.

Table S6. Variation of angles of rhombohedral geometry of [4+4] metallomacrocyclic unit of the parent MOF (**1**) and the guest exchanged complexes.

Incorporated guest	α	β	γ	Space group	geometry
Parent MOF	55.12	124.88		Monoclinic C2/C	Rhombohedral
H_2O	55.06	123.96		Monoclinic C2/C	Rhombohedral
$CHCl_3$	53.67	126.33		Triclinin P-1	Parallelogram
CH_2Cl_2	53.39	126.61		Monoclinic C2/C	Rhombohedral
CCl_4	54.46	125.54		Monoclinic C2/C	Rhombohedral
DCE	52.40	127.60		Monoclinic C2/C	Rhombohedral
DBE	55.31	125.69		Monoclinic C2/C	Rhombohedral
Glycol	52.40	127.60		Monoclinic C2/C	Rhombohedral
PhH	56.96	123.04		Monoclinic C2/C	Rhombohedral
$PhCH_3$	56.62	123.38		Monoclinic C2/C	Rhombohedral
o-$PhCl_2$	56.67	123.33		Monoclinic C2/C	Rhombohedral
$PhNH_2$	54.13	125.87		Triclinic *P-1*	Parallelogram
$PhCH_2NH_2$	55.84	124.16		Monoclinic C2/C	Rhombohedral
Naphthalene	56.66	122.57	57.81	Monoclinic $P2_1/C$	

Table S7. Variation of edge lengths of rhombohedral geometry of [4+4] metallomacrocyclic unit of the parent MOF (**1**) and the guest exchanged complexes.

Incorporated guest	a	b	c	d	Space group	geometry
Parent MOF	13.467				Monoclinic C2/C	Rhombohedral
H_2O	13.456				Monoclinic C2/C	Rhombohedral
$CHCl_3$	13.023	13.871			Triclinic P-1	Parallelogram
CH_2Cl_2	13.450				Monoclinic C2/C	Rhombohedral
CCl_4	13.590				Monoclinic C2/C	Rhombohedral
DCE	13.523				Monoclinic C2/C	Rhombohedral
DBE	13.451				Monoclinic C2/C	Rhombohedral
Glycol	13.420				Monoclinic C2/C	Rhombohedral
PhH	13.487				Monoclinic C2/C	Rhombohedral
$PhCH_3$	13.415				Monoclinic C2/C	Rhombohedral
o-$PhCl_2$	13.423				Monoclinic C2/C	Rhombohedral
$PhNH_2$	13.488	13.980			Triclinic P-1	Parallelogram
$PhCH_2NH_2$	13.491				Monoclinic C2/C	Rhombohedral
Naphthalene	13.564	13.564	13.317	13.317	Monoclinic $P2_1/C$	

Topological analysis after inclusion of different guests in 1D nanoporous channel of the parent MOF: Upon inclusion of different guests, there is no significant change in topology. But the pore size of the parent MOF changes showing breathing behavior according to size of the guests. We have analyzed the pore breathing by considering four Cu_2I_2 units connected with four ligands as a rhombus and subsequent change has been observed in edge lengths and angles of the rhombus.

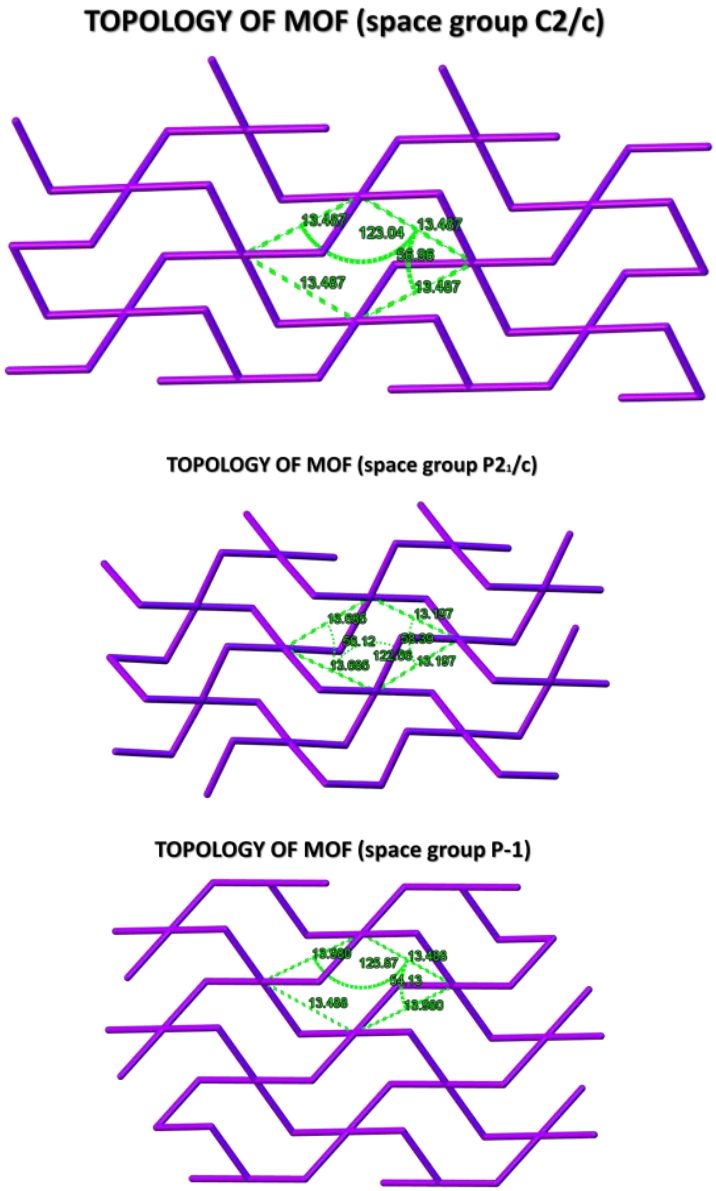

Figure S42. Topological analysis of the guest exchanged complexes with different space group.

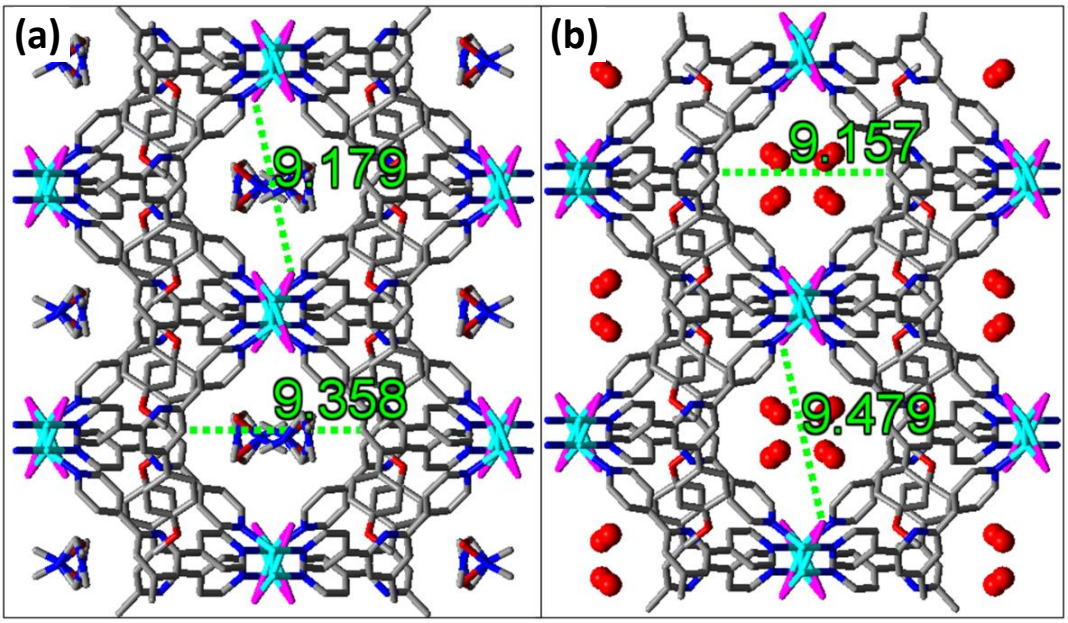

Figure S43. Variation of hydrophilic and hydrophobic pore dimention of the intermediate (a) Cu(I)MOF (**1**) (b) (**H_2O@Cu(I)MOF** (**1z**)) prior to guest inclusion which is induced by vapors of the guests**.**

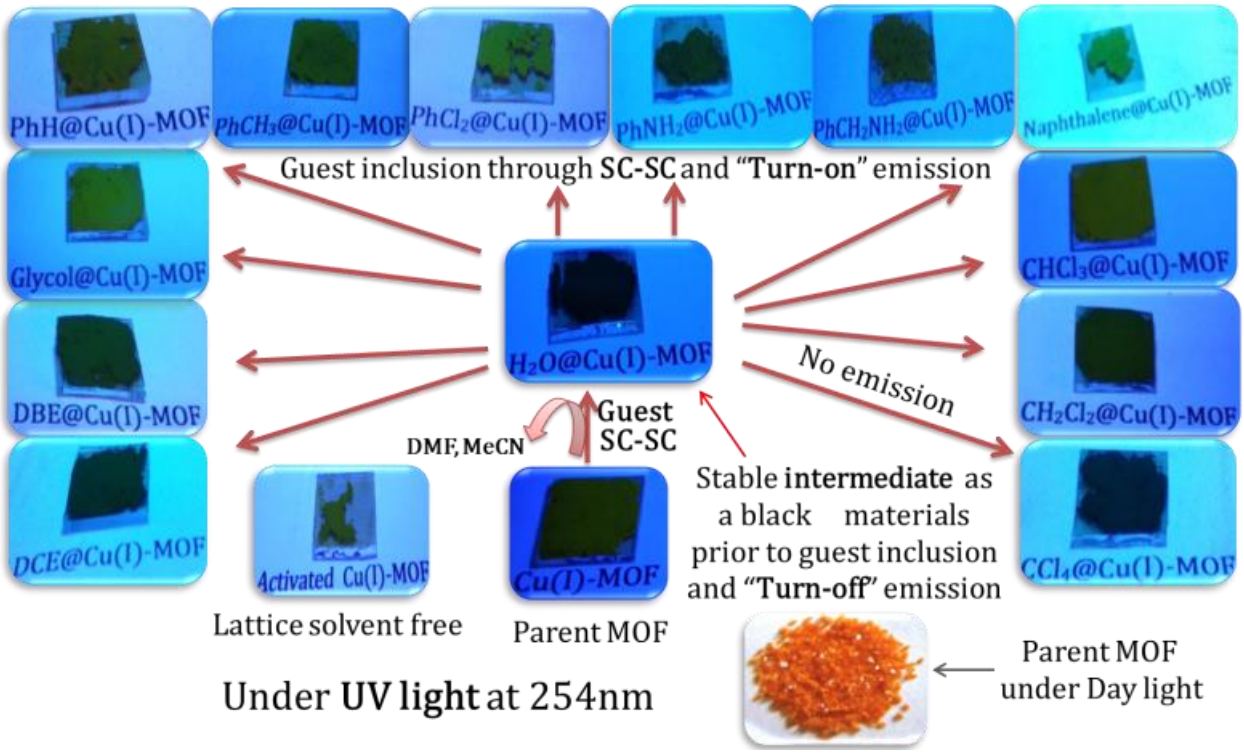

Figure S44. Parent MOF and its guest exchanged complexes under UV light at 254nm.

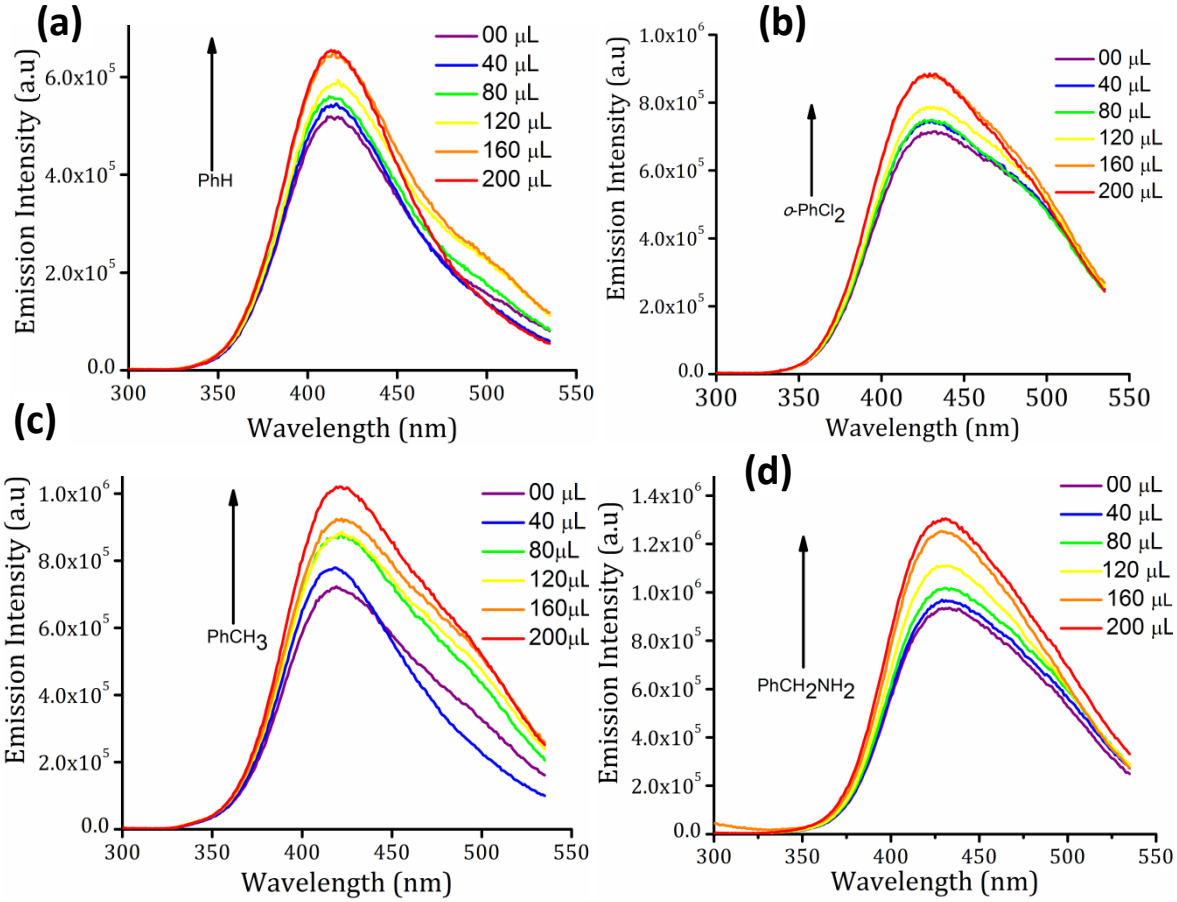

Figure S45. Emission spectra of **1** dispersed in dry MeCN upon incremental addition of MeCN solution of (a) PhH (b) *o*-$PhCl_2$ (c) $PhCH_3$ (d) $PhCH_2NH_2$ (1mM) at room temperature.

Table S8. Detection limit of different analytes

Analytes	Detection limit (mM)
PhH	0.0081
$PhCH_3$	0.006
o-$PhCl_2$	0.0097
$PhNH_2$	0.0046
$PhCH_2NH_2$	0.010